ARMY RESEARCH LABORATORY

A FOUR-DIMENSIONAL, MESOSCALE, NON-GAUSSIAN MULTISPECTRAL SMOKE MODEL

SBIR PHASE I FEASIBILITY STUDY

R. J. Yamartino, D. G. Strimaitis,
J. S. Scire, and E. M. Insley

Sigma Research Corporation
234 Littleton Road, Suite 2E
Westford, MA 01886

Under Contract DAAD07-91-C-0133
Contractor Monitor Frank V. Hansen

ARL-CR-15 *December 1992*

NOTICES

Disclaimers

The findings in this report are not to be construed as an official Department of the Army position, unless so designated by other authorized documents.

The citation of trade names and names of manufacturers in this report is not to be construed as official Government indorsement or approval of commercial products or services referenced herein.

Destruction Notice

When this document is no longer needed, destroy it by any method that will prevent disclosure of its contents or reconstruction of the document.

REPORT DOCUMENTATION PAGE

Form Approved
OMB No. 0704-0188

1. AGENCY USE ONLY (Leave blank)	2. REPORT DATE	3. REPORT TYPE AND DATES COVERED
	December 1992	Final

4. TITLE AND SUBTITLE

A FOUR-DIMENSIONAL, MESOSCALE, NON-GAUSSIAN MULTISPECTRAL SMOKE MODEL, SBIR PHASE I FEASIBILITY STUDY

5. FUNDING NUMBERS

61102/B53A (6.1)

6. AUTHOR(S)

R. J. Yamartino, D. G. Strimaitis, J. S. Scire, and E. M. Insley

7. PERFORMING ORGANIZATION NAME(S) AND ADDRESS(ES)

Sigma Research Corporation
234 Littleton Road, Suite 2E
Westford, MA 01886

8. PERFORMING ORGANIZATION REPORT NUMBER

ARL-CR-15

9. SPONSORING/MONITORING AGENCY NAME(S) AND ADDRESS(ES)

U.S. Army Research Laboratory
Battlefield Environment Directorate
White Sands Missile Range, NM 88003-5501

10. SPONSORING/MONITORING AGENCY REPORT NUMBER

11. SUPPLEMENTARY NOTES

Frank V. Hansen (Contract Monitor)

12a. DISTRIBUTION/AVAILABILITY STATEMENT

Approved for public release; distribution unlimited.

12b. DISTRIBUTION CODE

13. ABSTRACT *(Maximum 200 words)*

The feasibility of developing a four-dimensional, non-Gaussian mesoscale multispectral smoke model that could run on a personal computer is investigated. Several of the model components are formulated, coded, and tested, including the main driver program for accessing and interpolating the mesoscale winds and generating particle trajectories, a sub-grid-scale velocity field generator based on the kinematic simulation approach, and a dry deposition model for particle deposition velocities. Current understanding of flow and turbulence modeling is reviewed and can be applied to developing appropriate kinematic simulation fields. Technical approaches to account for the height and particle size dependent probability of particle removal and to compute the point and path average particle concentrations are also presented. Conclusions and recommendations for future work are included.

14. SUBJECT TERMS

Dispersion models, air pollution, atmospheric turbulence, smoke dispersion

15. NUMBER OF PAGES

71

16. PRICE CODE

17. SECURITY CLASSIFICATION OF REPORT	18. SECURITY CLASSIFICATION OF THIS PAGE	19. SECURITY CLASSIFICATION OF ABSTRACT	20. LIMITATION OF ABSTRACT
Unclassified	Unclassified	Unclassified	SAR

ACKNOWLEDGMENTS

We are grateful to Professor Julian C. R. Hunt and Dr. Richard Perkins of the University of Cambridge for their consultations on and insights into kinematic simulation, and to Dr. Lütz Janicke of Überlingen, Germany, for illuminating discussions regarding his LASAT-C model.

CONTENTS

ILLUSTRATIONS

TABLE

FIGURES

1. INTRODUCTION

1.1 Identification of the Problem

The U.S. Army currently has the need for the capability of rapidly modeling and evaluating the multispectral obscuration capacity of a smoke cloud in space and time. Such a multispectral smoke obscuration model requires that the fate of a number of particle size regimes be accounted for explicitly, as the scattering cross section of a smoke particle at a specific incident wavelength depends strongly on the particle's diameter. The further constraints that these simulations include realistic three-dimensional mesoscale structures of the flow and turbulence fields, as well as resolve the time dependence of the obscuring cloud's behavior on "relevant" time scales, suggest a model of substantial sophistication and computational intensity. Nevertheless, a further objective is to perform such modeling using the rather modest resources of a modern personal computer (PC).

1.2 Development of an Approach

A typical mesoscale wind field model may cover a lateral domain of 20 to 200 km with a typical resolution of from 500 m to 5 km and a vertical domain of up to 5 km with resolutions ranging from several meters near the surface to a kilometer or more near the top of the domain. Such spatial resolution is often far greater than the dimensions of the smoke cloud being modeled and, of course, only reflects those spatial structures in the flow having wavelengths greater than the resolution of the mesh. In addition, the temporal resolution of these wind fields is typically in the range of fractions of an hour (for example, 10 minutes) to one to several hours. Such time resolutions may be adequate to resolve the evolution of the mean flow but are clearly too coarse to resolve the influence of intermittent moderate size (for example, of the size order of the smoke cloud) sub-grid-scale eddies on the smoke cloud.

Two possible modeling approaches immediately come to mind--large eddy simulation (LES) and Monte Carlo Lagrangian particle dispersion. The high space-time resolution of an LES model could be used to drive a particle or Eulerian grid model; however, the required computational intensity of LES models calls for a supercomputer rather than a PC. Alternatively, one could use the wind field/boundary layer model's specification of the local turbulence fields to drive a Monte Carlo Lagrangian particle model. Such an approach generally considers each particle (or particle pair) to move independently and, therefore, leads to ensemble average concentration statistics, which for stationary turbulence can be considered equivalent to time-averaged concentrations. This relatively computationally inexpensive modeling approach is excellent for many applications but could yield misleading results in an environment where the issue of seeing and being seen may involve brief periods of time rather than time-averaged conditions.

A compromise approach might involve the use of "canned" sub-grid scale flow fields developed in advance with the aid of LES model simulations, combined with a Lagrangian particle model designed to let particles follow these large, yet sub-grid, scale motions augmented by a more traditional Monte Carlo trajectory component to account for smaller, unresolved scale eddies. Such an approach has

also been suggested by Sakai et al. (1991), and makes use of the rapidly evolving discipline of kinematic simulation. This methodology will serve as the basis for moving particles within the proposed model.

Of course, it is not enough to simply move the particles correctly; we must also account for their size-dependent removal rates and determine cost effective ways to assess local particle concentrations and path-averaged measures. Both of these issues can have very large computing cost implications for a model. For example, particles which are effective scatterers in the far infrared (IR) (for example, particle diameter d $\approx$ wavelength l $\approx$ 100 μ) can settle out with deposition velocities of order 10 cm/s whereas optimal ultraviolet (UV) scatterers can have deposition velocities ranging from 10^{-3} to 10^{-1} cm/s but all negligible relative to turbulent velocities of order 5-50 cm/s. Thus, it may be possible to simulate all particle sizes relevant to the UV transmission problem with a single mathematical particle whereas the IR transmission problem may require separate computation of trajectories of particles in the various size ranges. A truly comprehensive multispectral model might therefore require a choice (that is, user or model selected) of wavelength operational modes to avoid excessive calculation (for example, one mathematical particle for each physical particle size range) when a simpler calculation is adequate.

Choice of an appropriate particle counting methodology for concentration evaluation is also essential in balancing the cost of increased number of particles with the statistical uncertainties associated with too few particles. The proposed model will incorporate a modified "kernel estimator" that diffuses either the receptor location over a time-independent length scale or the point particles over a time-dependent scale corresponding to the root mean square (rms) separation generated by the unresolved fine scale eddies.

1.3 Overall Model Design

Figure 1 displays the basic modules making up the envisioned multispectral smoke dispersion model and the relationship of this model to external data files and the typical user. Perhaps the most important input data involves the three-dimensional gridded mesoscale wind fields and accompanying two-dimensional fields specifying boundary layer quantities of interest (for example, mixed layer depths, friction velocities, heat fluxes, convective velocity scale). These data are provided by a wind field/PBL model external to and separate from the dispersion model. While the current prototype accesses data produced by the CALMET meteorological model (Scire et al., 1990), there are few obstacles in substituting this model with one potentially more suitable to the Army's needs.

The principal user interface via a user control file will ensure relatively uncomplicated, straightforward use of the model. The user will need to specify the parameters associated with the proposed smoke release (for example, release locations, release quantities, and proposed sampling locations or transmission paths of interest). Supplementary detailed information, such as specification of the initial spectral profile of the smoke release, will be included in additional data files prepared well in advance of actual applications.

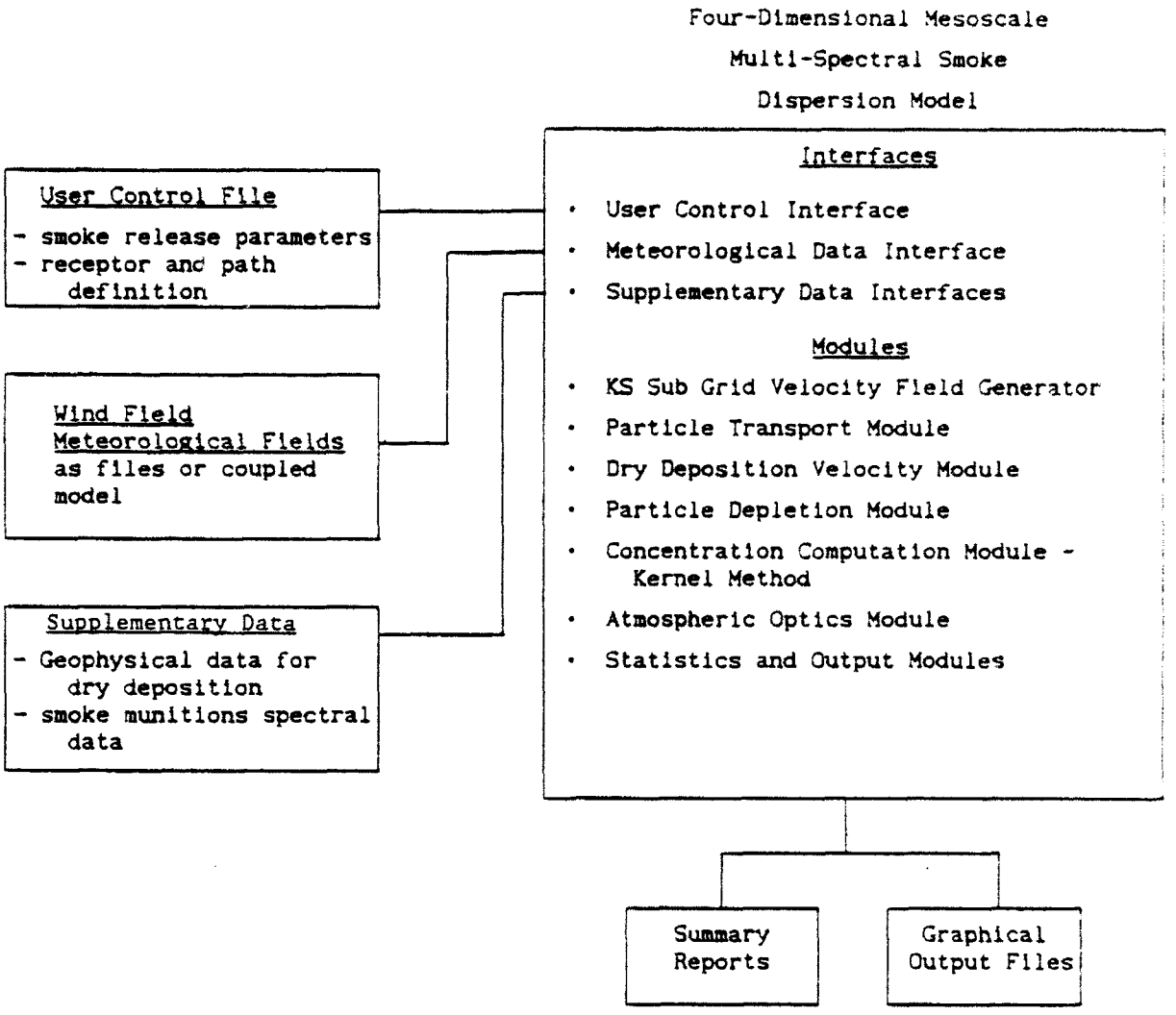

Figure 1. Overall model design.

1.4 Overview of the Technical Report

Section 2 of this report reviews the current status of mesoscale models of the flow and turbulence fields and describes how this information is incorporated into current formulations of Lagrangian particle models or the hybrid kinematic simulation/Langevin equation model envisioned here. Section 3 then deals with those aspects of the problem which involve the multispectral smoke aspects of the problem including the dry deposition module, adaptation of the dry deposition velocities to evaluate Lagrangian particle capture probabilities, and computation of the point and path averaged quantities of interest.

A number of the basic components needed for such a dispersion model have been coded and tested during the course of this project. These tests and preliminary evaluations are described in section 4.

Finally, the conclusions and recommendations resulting from this Phase I research and development effort are presented in section 5. A complete list of references is also provided.

2. MESOSCALE FLOW, TURBULENCE, AND LAGRANGIAN MODELING OF PARTICLE MOVEMENT

2.1 Overview of Mean Flow Models Incorporating Complex Terrain

A variety of wind field generators is currently available, ranging from analytic trajectory generators for specific terrain features, to objective analysis models, to diagnostic generators, and ultimately, to prognostic wind field generators of varying complexity. In the following subsections, we describe several of the more readily-available modeling approaches for each type of wind field generator.

2.1.1 Objective analysis models

Wind field models in this group use objective methods to create an entire grid of three-dimensional wind vectors from an irregular spatial distribution of measured two-dimensional vectors. This is typically done in two steps. Initially, wind vectors in the horizontal are specified at all points in the grid by interpolating among the measured wind vectors. Once this is completed, the second step makes use of procedures for modifying the vectors that were interpolated, with the aim of minimizing the divergence in the flow field. The influence of terrain is represented in boundary conditions that do not allow the flow to penetrate terrain features large enough to be resolved by the spacing of the grid in the horizontal. As such, these models create mass-consistent wind fields representative of the measured data, given the constraints imposed by the topography.

In a recent review article, Hunt et al. (1990), report that this modeling approach produces satisfactory results for scales of 5 km to 100 km, especially when wind data are obtained over length scales consistent with changes in surface topography. In fact, if the observed wind data sufficiently resolve important features of the flow, then the objective analysis method is likely to provide the most realistic, and the most cost effective means of estimating the wind field throughout the modeling region.

Two well-known objective analysis procedures are described by Sherman (1978) and Goodin et al. (1980). The first procedure, known as MATHEW (Mass-Adjusted Three-Dimensional Wind Field), develops a three-dimensional mass-consistent wind field by means of a variational calculus approach. The coordinate system is a fixed grid which does not follow terrain. Terrain is represented in the form of obstacle cells which impose vertical boundaries through which no flow is allowed. In step 1 of the procedure, interpolation of winds measured near the surface use $1/r^2$ weighting, while a synoptic analysis must be used to provide the wind field aloft. Goodin et al. (1980) point out that their method incorporates a terrain-following coordinate system with variable spacing in the vertical. Interpolation at the surface makes use of $1/r^2$ weighting, whereas winds, temperatures, and mixing heights in the upper layers make use of $1/r$ weighting. Large-scale terrain imposes barriers to the interpolation. The influence of smaller-scale terrain (less than one grid cell length) is included by solving Poisson's equation for a forcing function that is based on the thickness of the grid-layer, and terrain gradients. In the example application, Goodin et al. (1980) indicate that their method is faster than MATHEW, but results in larger horizontal divergence, and therefore larger estimates of vertical velocity.

2.1.2 Diagnostic models

Diagnostic models are similar to the objective analysis models in that they rely heavily on observed winds in order to obtain satisfactory estimates of the wind field throughout the modeling domain. However, in addition to the requirement that the modeled wind field be mass-consistent, they typically introduce other information about the likely structure of the wind field through use of diagnostic equations.

Endlich et al. (1982) describe a diagnostic model that makes use of the MATHEW method for reducing divergence. They introduce geostrophic winds above the boundary layer, and employ a logarithmic vertical profile to interpolate winds between the geostrophic wind at the top of the boundary layer and the surface winds. They cast the continuity equation in a terrain-following coordinate system, and formulate the Lagrange multiplier relations. By neglecting some terms that may be significant in areas of steep terrain, the system becomes analogous to Sherman's (1978), so the MATHEW method may be used. This approach essentially incorporates the influence of terrain on the flow by imposing the depth of the boundary layer over the terrain, and forcing the flow within the boundary layer to satisfy the continuity equation.

A second type of diagnostic wind field model is described by Douglas and Kessler (1988). Although it uses the Goodin et al. (1980) method for minimizing divergence, it first includes diagnostic equations for estimating kinematic effects of the terrain, slope flows, and blocking effects of terrain in the presence of a stable density stratification. A mean wind for the region, obtained from upper-air information, is used to compute the vertical velocity associated with terrain features, in a terrain-following coordinate system (Liu and Yocke, 1980). The divergence-minimization procedure is then applied to modify the initial mean wind field. Slope flows estimated by procedures suggested by Allwine and Whiteman (1988) are then added to the field. Finally, if the local Froude number at a grid point is less than a critical value, the flow at the grid point must not have an uphill component. If it should have an uphill value, the vector is turned so that it is tangential to the height-contour of the terrain. This stipulation simulates the largely horizontal flow observed below a "critical dividing-streamline."

Once this flow-field is complete, it embodies several terrain-induced features that may or may not be represented in the observed wind field. The second step in this procedure introduces the observed wind data. Values of the windspeed at grid points near monitoring stations are highly influenced by the observed winds. However, grid points that are relatively far from monitoring stations retain the characteristics imposed by the diagnostic relations. After smoothing to reduce discontinuities, and adjustments to limit the vertical velocity at the top of the domain, the divergence minimization procedure of Goodin et al. (1980) is applied to obtain the mass-consistent wind field. The recently developed CALMET model (Scire et al., 1990) incorporates the Douglas and Kessler (1988) diagnostic model together with a complete model for the PBL and micrometeorological quantities.

Several recently developed diagnostic wind field models also incorporate the concept of a dividing-streamline or Froude number in their formulation in order to better represent blocking or channeling effects of terrain during periods with stably-stratified density profiles in the vertical. NUATMOS (Ross et al., 1988)

is an adaptation of ATMOS1 (Davis et al., 1984) which is based on a variational calculus method similar in concept to MATHEW. However, NUATMOS makes use of terrain-following coordinates, and includes a method for prescribing the parameter α, which controls the adjustments made to the vertical winds relative to the horizontal winds, by means of the local Froude number. Ross et al. (1988) demonstrate the ability of NUATMOS to characterize potential flow solutions for flow over simple isolated features where $\alpha = 1$, and discuss the success of several approaches to formulating the α parameter in terms of the Froude number by comparing results with tow-tank results obtained by Hunt and Snyder (1980). When $\alpha = 0$, the divergence in the flow-field is minimized by altering only the horizontal winds. By equating this limit with the low Froude number regime, a largely two-dimensional flow is obtained. Because a local Froude number is used for each layer in the model, the method can result in channeled, two-dimensional flow in the lower layers, and nearly potential flow in the upper layers.

The WOCSS (Winds on Critical Streamline Surfaces) method developed by Ludwig and Endlich (1988) takes a substantially different approach to incorporating channeling effects that result from stratification. This approach constrains the analysis by defining coordinate surfaces that represent surfaces through which no flow is allowed. These coordinate surfaces may intersect the terrain, and are determined objectively by essentially allowing a vertical deflection caused by terrain to be no greater than the local length scale, U/N. This means that coordinate surfaces will intersect terrain whenever the flow cannot pass over the terrain. Winds at grid points that end up "inside" the terrain are set to zero, thereby forcing the flow outside of the terrain to travel around the terrain because within each layer no divergence is allowed. This method essentially turns the three-dimensional flow problem into a number of two-dimensional flow problems. Mass fluxes are adjusted to satisfy the continuity equation by means of the procedure described by Endlich (1967), except that vorticity constraints are not imposed.

Ludwig et al. (1991) point out that this WOCSS method does not provide sufficient guidance for defining coordinate surfaces in the absence of stable stratification. Unlike the methods based on the MATHEW approach, it does not provide flow fields similar to potential flow in the absence of stratification. They suggest that further development of the method might include combining it with a two-dimensional prognostic model to produce realistic vertical profiles of winds and temperatures which can be treated as "observations." Such an approach would introduce diabatic effects such as drainage flows and coastal circulations.

2.1.3 Analytic flow models

When complex flow fields must be resolved on scales of order 1 km or less, with few wind measurements available, Hunt et al. (1990) suggest that interpolative approaches like objective or diagnostic procedures cannot be relied upon. In their place, they advocate the use of what we will call analytic flow models. These approaches typically use scale analyses to simplify the equations of motion within regions that are important to the dynamics governing the flow. These regions are then combined using the methods of matched asymptotics; that is, solutions for different regions must match at the interface and have similar characteristics at infinity.

In a recent review paper, Carruthers and Hunt (1990) describe various flow regimes associated with terrain, identifying major dimensionless parameters that are able to classify, or order, these regimes (after Hunt and Richards, 1984; Snyder, 1985). They consider stratification effects (neutral-to-stable), rotation effects, and changes in roughness. However, they do not consider katabatic effects such as drainage flows at night or flows resulting from differential heating during the day.

The modeling approach to these flows is based upon linear analysis. That is, the presence of terrain merely perturbs the flow, so that perturbation velocities are small compared to the mean flow. Upon making this assumption, linearized versions of the governing equations can be solved analytically. The most complete approach of this type is the linear three-dimensional theory of Hunt et al. (1988). Carruthers and Hunt (1990) point out that this is based on earlier works of Jackson and Hunt (1975) and Townsend (1966). Two regions are defined--an inner region in which changes in shear stress are important, and an outer region in which the flow can be treated as inviscid. The depth of the inner region (ℓ) is given by the implicit relation

$$\ell \ln (\ell/z_o) = 2 k^2 L \qquad (1)$$

where z_o is the surface roughness length, k is von Karman's constant, and L is the length scale of the hill (see figure 2). Throughout the inner region, the turbulence is assumed to be in local equilibrium. A thin surface layer allows the solution to be matched to the surface boundary conditions. The outer region is composed of two layers; a middle layer and an outer layer. Shear in the approach flow dominates the solution for the middle layer. The solution in the outer layer characterizes the response of the fluid to the underlying perturbations. The perturbations decay with height if the stratification is very weak (potential flow solutions are obtained), and the perturbations produce waves for moderate to strong stratification.

The solutions for the perturbation velocities in the two regions are obtained for arbitrary terrain by representing the terrain by its Fourier transform. However, the basic assumption that the perturbations are small compared to the incident flow requires that the terrain be characterized by small slopes, so that the use of "arbitrary" terrain must be qualified accordingly. The most general numerical model that is based on these methods is FLOWSTAR (Carruthers et al., 1988). Carruthers and Hunt (1990) point out that the use of Fast Fourier Transforms (FFT's) allows rapid computations to be made, and since the method is analytic, the flow field may be found at precise locations, rather than within a grid. They also point out that perturbations due to changes in roughness and terrain slope can be summed, since the analysis is linear.

This method applies to flow over terrain which does not possess steep slopes, for meteorological conditions that can be characterized by relatively simple profiles of windspeed and temperature in the vertical. If the stratification is strong (that is, the Froude number $u/NH < 1$) these methods are not applicable. As discussed in connection with the diagnostic models, the flow tends to be two-dimensional in a layer below the critical dividing-streamline. This means that perturbations are as large as the incident flow in this layer, which invalidates the model. For general application, the FLOWSTAR approach would have to incorporate a complementary model in order to treat this aspect of the flow. Note,

however, that the flow above the critical dividing-streamline height behaves as a weakly stratified flow, so that the outer region solutions might be adapted to model this region.

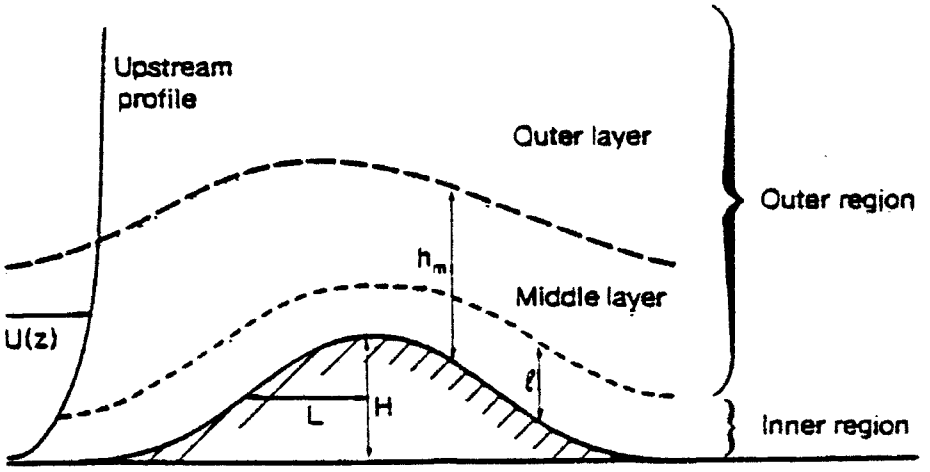

Figure 2. Flow regions for the linear analysis (Carruthers and Hunt, 1990).

2.1.4 Prognostic flow models

Prognostic models used to simulate mesoscale flows in complex terrain were recently reviewed by Pielke (1989), and summarized by Pielke et al. (1990). Seven distinct models developed and applied in North America were included in the review. Of these, four were found to be applicable to complex terrain--the MASS model, the NCAR/Penn State (MM4) model, the CSU RAMS model, and the Los Alamos model HOTMAC (Yamada and Bunker, 1988). Each of these includes a primitive equation framework, a nested grid, and each makes use of the hydrostatic approximation. Only CSU RAMS also includes a nonhydrostatic option. The minimum spacing allowed for the horizontal grid varies among these models. CSU RAMS can accept a spacing of about 100 m; the Los Alamos model has a minimum spacing of 380 m; MM4 has a minimum of about 1000 m; and MASS requires a horizontal spacing of at least 7000 m.

The four models that are readily applicable to complex terrain include, in principle, a complete description of the mean flow field, including diabatic effects. However, by their very nature, they require significant computer resources. Most simulations make use of super computers, but "super-mini" or graphics super-workstations appear to be viable alternatives. In a recent demonstration project, Mattocks et al. (1989) adapted MASS for execution on an Alliant FX-1 minisupercomputer, with satisfactory results. Their tests indicate that the minisupercomputer ran at approximately 1/20th the speed of a CRAY 2 supercomputer, which is about three times the anticipated speed.

2.2 Turbulence Characterization Approaches and Parameterizations

The various flow field modeling approaches outlined in section 2.1 characterize turbulence in the flow in several ways. The objective analysis and the diagnostic methods do not rely on characterizing the turbulence at all, and at most

include estimates of turbulence in an ad-hoc manner if diffusion estimates are required. In such a case, the turbulence may simply be parameterized in terms of a Pasquill stability class index, or it may be explicitly related to micrometeorological parameters. The point is that the turbulence is derived from mean properties of the flow field--the flow field itself is determined without regard for the effect of turbulence.

Analytic flow field models do incorporate aspects of the turbulence in modeling the mean flow. This is done primarily in the inner region, where turbulence is in local equilibrium. Essentially, both the shear stress due to the mean flow and the perturbation shear stress are explicitly contained in the linearized equations of motion. These shear stresses are typically characterized in terms of a mixing length formulation.

The prognostic models also explicitly incorporate models for turbulent transport, which make up an integral part of the system of equations used to obtain the mean flow field. Depending on the type of closure employed, the turbulence is modeled in terms of a gradient transfer with specified eddy coefficients (K-Theory), or by formulating the Reynolds stresses explicitly, and closing the system of equations with a model for the higher-order products of the turbulent velocity fluctuations (for example, second-order closure). The MASS and NCAR/Penn State models use first-order closure, the Los Alamos model uses second-order closure, and the CSU RAMS model includes an option to use either.

Other efforts to model atmospheric turbulence are found in the literature, although these have not been coupled to wind field models suitable for applications in complex terrain. Two such approaches are LES (Large Eddy Simulation) and KS (Kinematic Simulation). LES is an approach in which a modified form of the Navier-Stokes equation is solved on a grid sufficiently small to resolve the eddies of interest. Subgrid-scale motions are parameterized, and must generally be small enough to lie with the inertial subrange. LES models similar to Deardorff (1974) for the convective boundary layer use gradient transfer equations for subgrid-scale exchange, and include an equation for the energy of these motions. As a result, LES results for the stable boundary layer may be significantly influenced by the particular parameterization used for subgrid scale processes.

KS is a recently proposed method for simulating the details of a turbulent velocity field with prescribed spectral properties. As KS theory begins with an analytic Fourier representation, it is not tied to a computational grid. However, it contains no dynamics, so that the effects of vortex- stretching, for example, are represented only to the extent that the spectral properties embody the result of this process. Because of this, the KS approach may be viewed as a "repository" of present knowledge about Eulerian/Lagrangian statistics of turbulence. KS theory will be examined in greater detail in section 2.4.

In the remainder of this section, we present methods for characterizing turbulence variances (as σ_v and σ_w, for example) in undisturbed flows by means of established micrometeorological parameters, and we present related expressions for time scales. Approximate expressions for the spectra of turbulence are also discussed. Because flows are altered by the presence of terrain, properties of the turbulence are altered as well, and suggestions for how to formulate these changes are reviewed.

2.2.1 σ_v and σ_w

Many laboratory experiments, field studies, and numerical simulations (for example, Deardorff and Willis, 1975; Caughey, 1981; Lamb, 1981) have shown the importance and utility of convective scaling in the convective boundary layer. Convective scaling has been successfully applied to data collected at a wide variety of sites, including oceans, rural land surfaces (for example, Hicks, 1985) and urban areas (Ching et al., 1983). Similarly, in the stable boundary layer, local scaling has been shown to apply (for example, Hunt, 1981; Nieuwstadt, 1984).

Weil (1985) and Briggs (1985) provide reviews on the use of similarity theory in diffusion models. In the convective boundary layer, Weil describes the turbulence characteristics in three layers:

(1)	Surface layer - $z \leq 0.1$ h;	σ_v - constant with height σ_w increases with height
(2)	Mixed layer - $0.1h < z < 0.8h$;	σ_v - constant with height σ_w - constant with height
(3)	Entrainment layer - $z > 0.8h$;	σ_v decreases with height σ_w decreases with height

In the surface layer, Panofsky et al. (1977) propose the following relations.

$$\sigma_v = u_* \left[4 + 0.6\,(-h/L)^{2/3}\right]^{1/2} \tag{2}$$

$$\sigma_w = u_* \left[1.6 + 2.9\,(-z/L)^{2/3}\right]^{1/2} \tag{3}$$

where u_* is the surface friction velocity (m/s), and L is the Monin-Obukhov length (m).

Hicks (1985) suggests the following for the mixed layer (0.1 to 0.8 h).

$$\sigma_v = \left(3.6\ u_*^2 + 0.35\ w_*^2\right)^{1/2} \tag{4}$$

$$\sigma_w = \left(1.2\ u_*^2 + 0.35\ w_*^2\right)^{1/2} \tag{5}$$

In the neutral boundary layer, Arya (1984) reports monotonically decreasing values of σ_v and σ_w throughout the mixed layer. Using the Blackadar and Tennekes (1968) relationship for the neutral boundary layer height, Arya's results can be expressed as:

$$\sigma_v = 1.5 \exp(-0.9\ z/h) \tag{6}$$

$$\sigma_w = 1.3 \exp(-0.9\ z/h) \tag{7}$$

In the stable boundary layer, Nieuwstadt (1984) finds that σ_v and σ_w bear constant ratios with the local friction velocity.

$$\sigma_v/u_{*\ell} = C_v \tag{8}$$

$$\sigma_v/u_{*\ell} = C_w \tag{9}$$

where $u_{*\ell}$ is the local friction velocity (m/s), and, C_v and C_w are constants.

Hanna et al. (1986) suggest that $C_v \simeq 1.6$. C_w has a value $\simeq 1.3$ (Nieuwstadt, 1984). The local friction velocity, $u_{*\ell}$, can be expressed (Nieuwstadt, 1984) as:

$$u_{*\ell} = u_* \ (1 - z_h)^{3/4} \tag{10}$$

2.2.2 Lagrangian time scale

Empirical equations for the Lagrangian time scale have been proposed by Hanna (Nieuwstadt and Van Dop, 1982) for use in Monte Carlo particle modeling. He also presents expressions for σ_v and σ_w, and for σ_u. Although these expressions differ from those presented above, we point out that he equates σ_u with σ_v for the convectively unstable boundary layer, and equates σ_v with σ_w for the neutral and stable stratified boundary layer. For the latter, σ_u is given as:

$$\sigma_u = 2.0\ u_* \left(1 - \frac{z}{h}\right) \qquad (stable) \tag{11}$$

$$\sigma_u = 2.0\ u_* \exp(-3\ f\ z/u_*) \qquad (neutral) \tag{12}$$

where f is the coriolis parameter. The Lagrangian time scales proposed by Hanna are:

Convectively Unstable Boundary Layer

$$T_{L_a} = T_{L_c} = 0.15\ h/\sigma_v \tag{13}$$

$$z < 0.1h;\ z - z_o > -L:\quad T_{L_z} = \frac{0.1\ z/\sigma_w}{0.55 + 0.38\ (z - z_o)/L} \tag{14}$$

$$z < 0.1h;\ z - o < -L:\quad T_{L_z} = 0.59\ z/\sigma_w \tag{15}$$

$$z > 0.1h:\quad T_{L_z} = 0.15\ \frac{h}{\sigma_w}\left(1 - \exp\left(-5\frac{z}{h}\right)\right) \tag{16}$$

Stably Stratified Boundary Layer

$$T_{L_a} = 0.15\ \frac{h}{\sigma_u}\left(\frac{z}{h}\right)^{0.5} \tag{17}$$

$$T_{L_c} = 0.07\ \frac{h}{\sigma_v}\left(\frac{z}{h}\right)^{0.5} \tag{18}$$

$$T_{L_z} = 0.10\left(\frac{z}{h}\right)^{0.8} \tag{19}$$

Neutral Boundary Layer

$$T_{L_a} = T_{L_c} = T_{L_z} = \frac{0.5\ z/\sigma_w}{1 + 15\ f\ z/u_*} \tag{20}$$

In these expressions, the subscript "a" denotes a quantity describing fluctuations along the flow, and "c" denotes a quantity describing crosswind fluctuations. We use the alternate notation in which "u" is along the flow, and "v" is across the flow (horizontal) in describing σ_u and σ_v, and for σ_w.

2.2.3 Velocity spectra

Following the work performed by Kaimal et al. (1972, 1976) and Kaimal (1973) in characterizing velocity spectra, several authors have developed revisions which extend the expressions to greater heights above the surface. For the convective boundary layer, Hojstrup (1982) has developed expressions that are valid throughout the lower half of the layer, and that smoothly approach the neutral behavior found in the Kansas data (Kaimal et al., 1972). More recently, Moraes (1988) extended Kaimal's (1973) formulas for the stably stratified surface layer to the upper part of the boundary layer by incorporating Nieuwstadt's (1984) local similarity scaling. The remaining area in which the representations may be inadequate is the upper half of the convective boundary layer. Hojstrup (1982) points out that spectra in this region are influenced by entrainment processes at the top of the layer, and the effect of the "lid" itself as a boundary that limits the vertical scale of motion.

2.2.3.1 Convective boundary layer (Hojstrup, 1982)

$$\frac{nS_u(n)}{u_{*_o}^2} = \frac{0.5f_i}{1 + 2.2(f_i)^{5/3}}\left(\frac{h}{-L}\right)^{2/3} + \frac{105f_{ru}(1 - z/h)^2}{(1 + 33\ f_{ru})^{5/3}\ (1 + 15z/h)^{2/3}} \tag{21}$$

$$\frac{nS_v(n)}{u_{*_o}^2} = \frac{0.95f_i}{(1 + 2f_i)^{5/3}}\left(\frac{h}{-L}\right)^{2/3} + \frac{17f_{rv}(1 - z/h)^2}{(1 + 9.5f_{rv})^{5/3}(1 + 2.8z/h)^{2/3}} \tag{22}$$

$$\frac{nS_w(n)}{u_{*_o}^2} = F(f, z/h)\ \frac{0.95f_i}{(1 + 2f_i)^{5/3}}\left(\frac{h}{-L}\right)^{2/3} + \frac{2f(1 - z/h)^2}{1 + 5.3(f)^{5/3}} \tag{23}$$

where n is the frequency in Hz and the reduced frequencies, f, are given as

$$\begin{aligned} f &= nz/u\ ;\ f_{ru} = f/(1 + 15z/h) \\ f_i &= nh/u\ ;\ f_{rv} = f/(1 + 2.8z/h) \\ f(f, z/h) &= \left[\frac{f^2 + (0.3z/h)^2}{f^2 + (0.15)^2}\right]^{1/2} \end{aligned} \tag{24}$$

Also, h is the height of the lowest inversion, L is the Monin-Obukhov length, and u_{*_o} is the friction velocity in the surface layer.

Such analyses based on observed data from the convective boundary layer can be significantly augmented by simulation data bases produced by LES models. The data base and analyses performed by Moeng and Wyngaard (1988) should greatly facilitate a comprehensive modeling of the CBL.

2.2.3.2 Neutral/stable boundary layer (Moraes, 1988)

The velocity spectra in the surface layer follow Kaimal (1973), as recast by Moraes and Epstein (1987):

$$\frac{nS_i(n)}{u_*^2\phi_\varepsilon^{2/3}} = \gamma_i \frac{0.164f}{f_{oi}^{5/3} + 0.164f^{5/3}} \tag{25}$$

where i denotes one component of the turbulence (u,v,or w), f = nz/u, and f is the dimensionless dissipation rate for turbulent energy. The parameter γ_u has the following values:

$$\gamma_u = 0.3$$

$$\gamma_v = 0.4$$

$$\gamma_w = 0.4$$

The reference value for the frequency scale is given by

$$f_{oi} = \beta_i[1 + 2.5(z/l)^{3/5}]^{3/2} \tag{26}$$

where i again denotes one of the components u, v, or w. The parameter β_i has the following values:

$$\beta_u = 0.012$$

$$\beta_v = 0.045$$

$$\beta_w = 0.094$$

Above the surface layer, Moraes (1988) retains the functional form of spectra in the surface layer, but incorporates results from local similarity theory. The resulting equation for the velocity spectra is

$$\frac{nS_i(n)}{U_*^2\Phi_\varepsilon^{2/3}} = \frac{0.164f}{(f_{oi}^{SBL})^{5/3} + 0.164f^{5/3}} \tag{27}$$

where U_* is the local turbulence velocity scale, f_{oi}^{SBL} is the reference value for the frequency scale in the stable boundary layer, Φ_ϵ is the dimensionless energy dissipate rate in the stable boundary layer:

$$\Phi_\epsilon = 1.2(1 + 3.7z/\Lambda) \tag{28}$$

and γ_i and f are the same as in the surface layer. The local scaling length Λ is related to the stable boundary layer (h) and the Monin-Obukhov length (L) for the surface layer. Following Nieuwstadt (1984), Moraes finds that

$$\Lambda = (1 - z/h)^{5/4} L \tag{29}$$

Furthermore, the frequency scale for the stable boundary layer is given by

$$f_{oi}^{SBL} = \beta_i^{SBL}(1 + 3.7\ z/\Lambda) \tag{30}$$

where

$$\beta_i^{SBL} = \beta_i \frac{[1 + 0.628(h/L)^{3/5}]^{3/2}}{1 + 0.422(h/L)} \tag{31}$$

Values for the parameter β_i are the same as those in the surface layer.

The recent data reported by Smedman (1991) should also improve characterization of the spectra in the SBL.

2.2.4 Changes induced by terrain

Carruthers and Hunt (1990) provide an overview describing how changes in the mean flow over hills also affects the properties of turbulence. In essence, they state that the turbulence is in near equilibrium with the altered flow in the inner region near the surface of the hill, and the turbulence in the outer region is changed by the distortion of the mean flow. The two regions, inner and outer, largely conform to the inner and outer regions referred to in figure 2.

In the inner region, the turnover time scale for the eddies is of order z/u_*, which is less than the travel time over the hill. Consequently, the turbulence in the flow has time to adjust to changes in the flow, and is therefore in approximate equilibrium with the flow. Therefore, fractional changes in the turbulence are equal to fractional changes in the shear stress:

$$\frac{\Delta \overline{u_i^2}}{\overline{u_i^2}} = \frac{\Delta \tau}{\tau} \tag{32}$$

Because the change in the shear stress decreases rapidly with height above the surface, it is found that the $\Delta\overline{u_1^2}$ decreases t nearly zero at one-third the depth of the inner region.

The turnover time increases with the size of the eddies and, therefore, with height, so that it exceeds the travel time over the hill for eddies in the outer layer. Here, changes in the flow field distort the eddies in the approach flow, and the effect can be modeled by rapid distortion theory as explained by Britter et al. (1981). Carruthers and Hunt (1990) report that Newley (1985) and Zeman and Jensen (1987) have found that anistropy in the upstream turbulence should be included, and suggested that

$$\frac{\Delta\overline{u_1^2}}{\overline{u_1^2}} = -\frac{6}{5}\left(1 - \frac{1}{3\ \overline{u_1^2}/\overline{u_3^2}}\right)\Delta S \tag{33}$$

$$\frac{\Delta\overline{u_3^2}}{\overline{u_3^2}} = -\frac{6}{5}\left(1 - \frac{\overline{u_1^2}/\overline{u_3^2}}{3}\right)\Delta S \tag{34}$$

where ΔS is the speed-up factor. This result applies for the special case in which $\overline{u_2^2} = \overline{u_3^2}$, where component 1 is along the flow, 2 is across the flow (lateral), and 3 is across the flow (normal to the terrain). Finnigan (1988) elaborates on the processes that are important between the inner and outer regions, which include curvature effects and nonlinear interactions as well as rapid distortion.

2.3 Overview of Monte Carlo Lagrangian Particle Modeling

In Lagrangian particle models, particles are moved in the Eulerian frame by the basic equation

$$\boldsymbol{x}(t + \Delta t) = \boldsymbol{x}(t) + [\underline{u}(\boldsymbol{x}, t) + \underline{u}'(\boldsymbol{x}, t)] \cdot \Delta t \tag{35}$$

where $\underline{u}(\underline{x},t)$ represents the space-time varying mean flow velocity, and $u'(x,t)$ is the stochastic vector component. Evolution of this stochastic component is then modeled as a first-order autoregressive or Markov process using Langevin stochastic differential equations (Gifford, 1982; Sawford, 1984),

$$du' = -u'dt/T_L + du'', \tag{36}$$

for each vector component and where T_L is the Lagrangian time scale and du" are the random velocity components arising from a white noise modeling of particle accelerations. Sawford (1991) discusses equation (36) in relation to lower and higher order autoregressive equations involving the particle's position (that is, random walk modeling) and acceleration, respectively.

The stochastic term u" is often reexpressed (for example, Rodean, 1991) as $(C_o\epsilon)1/2dW(t)$, where C_o is the universal constant for the Lagrangian structure, e is the turbulent kinetic energy dissipation rate and dW is an increment of a Wiener process having zero mean and a variance of dt.

In many applied models, the solution of equation (36) is expressed as

$$u'(t) = \alpha_u \cdot u'(t - \Delta t) + R \cdot \sigma_u \cdot \sqrt{1 - \alpha_u^2} + d_u \tag{37}$$

where $\alpha_u = \exp(-\Delta t/T_{Lu})$

T_{Lu} is the Lagrangian time scale for the u component,

R is a random Gaussian number having zero mean and unit variance,

σ_u is the standard deviation of u velocity fluctuations, and

d_u is the u component drift velocity.

Similar equations are used for the v' and w' wind components as well. The drift velocity can be shown to be a necessary ingredient to prevent buildup of particles in low turbulence regions and is specified by Sawford (1985) as

$$d_u = (1 - \alpha_u)\, T_{Lu} \cdot \frac{\partial \sigma_u^2}{\partial x} \cdot \left[(\sigma_u^2 + u^2)/(2\sigma_u^2) \right] \tag{38}$$

for the u component. Other authors (for example, Legg and Raupach, 1982; Ley and Thompson, 1983) model this drift velocity as effectively, but more simply, as

$$d_u = \Delta t \cdot \frac{\partial \sigma_u^2}{\partial x} \tag{39}$$

Equation (37) reduces to the random walk model in the limit $T_{Lu} \to 0$ and to a purely deterministic model as $T_{Lu} \to \infty$. Further, a moments analysis of this equation (37) shows that while it has a mean corresponding to the drift velocity, d_u, and variance corresponding to $(1 - \alpha_u^2)\sigma_u^2$, the third moment (or skewness)

vanishes. Thus, equation (37) is not directly appropriate to the modeling of convective conditions.

The somewhat more complex problem of skewed turbulent spectra is basically solved by selecting the random component, u", of equation (36) from the desired probability density function (pdf) of turbulent velocities. Weil (1990) provides a comprehensive review of such approaches as applied to modeling the convective boundary layer.

Another issue requiring modification of the Langevin formulation involves attempts to generate finite velocity cross correlations (for example, $\overline{u'w'} < 0$) rather than the zero cross correlations which result from the evolution of independent Langevin equations for the u', v', and w' components. Zannetti (1990) provides a review of such attempts and has included such cross correlations into his MC-LAGPAR II model (Zannetti, 1986). In our planned usage of Langevin equation models for only the shorter wavelength portion of the turbulent spectrum, it will not be necessary to add such cross correlation contributions as they will arise naturally from the flow fields specified via kinematic simulation.

Finally, we note that equation (35) is strictly appropriate for massless and inertialess particles that instantly adjust to the turbulent velocities. For particles with significant gravitational settling velocities, v_g, or inertia, equation (35) is replaced by the pair of vector equations

$$\underline{x}(t + \Delta t) = \underline{x}(t) + \underline{v}(\underline{x}, t) \cdot \Delta t \tag{40}$$

and

$$\frac{d\underline{v}}{dt} = \gamma(\underline{u}(\underline{x}, t) + \underline{u}'(\underline{x}, t) - \underline{v}(\underline{x}, t)) - \underline{g} \tag{41}$$

where

$\underline{v}(\underline{x},t)$ is the velocity of the particle,

$\underline{g} = (0,0,g)$ where g is the acceleration due to gravity, and

$\gamma = 1/\tau_p$ is the inverse of the particle response time τ_p.

Clearly as the particle response time goes to zero equation (41) has the solution, $\underline{v} = \underline{u} + \underline{u}'$, and equation (35) is recovered. For spherical particles governed by Stokes law, Squires and Eaton (1991) assume

$$\gamma = 18\mu/(\rho_p d^2) \tag{42}$$

where μ is the dynamic viscosity of air, ρ_p is the particle density, and d is particle diameter. Mallier and Maxey (1991) discuss the much more general equations applicable to nonspherical particles. Frost et al. (1982) use a potentially more generally expression for their MoCaPD model which reduces to

$$\gamma = \frac{3}{4} (\rho_a / \rho_p) C_d |V_a| / d , \tag{43}$$

where ρ_a is the density of air,

C_d is the drag coefficient defined as a function of particle Reynolds number, and

$|V_a|$ is the magnitude of the relative velocity of the particle in air.

However, a recent study by Hashem and Parkin (1991) suggests that the effects of particle inertia are negligible for particles up to 500 μm in diameter so that γ can be expressed in terms of the terminal velocity, v_t, of the particle and the turbulence parameters σ_w and T_{Lw} for the w component. This then leads to a closed form expression for the particle velocity.

2.4 Kinematic Simulation and Hybrid Theories

In the case of single particle Lagrangian trajectories, individual particle velocity components (u_i', v_i', w_i') evolve independently of one another and are uncorrelated with the velocity components of a neighboring particle. These characteristics of the particles' motions imply that the flow fields influencing a specific particle are not assured of being divergence free and that colocated particles are moving completely independently of one another. The first of these deficiencies can lead to the accumulation of particles in low turbulence zones: a problem that can be compensated for on average by introducing drift velocities. The second deficiency implies that such single particle, Monte Carlo Lagrangian trajectory modeling can only lead to ensemble average predictions and statistics.

The most logical way to avoid these compromises is to let the particles follow the actual turbulent flow fields present at any point in space and time. Such "actual" turbulent flow fields can either be generated by dynamical simulations (DS), involving solutions of the Navier Stokes equations over space and time, or by kinematic simulations (KS), involving the conjecture of flow fields which at a minimum obey the constraint $\underline{\nabla} \cdot \underline{V} = 0$ (or $\underline{\nabla} \cdot \rho \underline{V} = 0$).

DS methods encompass both the direct numerical simulation (DNS) and large eddy simulation (LES) methodologies and lead to a more complete description of the turbulent flow fields in the sense that all (or most) of the relevant physics is included. Such approaches are currently too computationally intensive for the intended application but can be utilized as an important resource to guide in the development of appropriate KS field properties and supplemental constraints.

KS theory begins with the representation of the vector flow field $\underline{u}(\underline{x},t)$ as a four-dimensional Fourier transform of an arbitrary amplitude function, $S(\underline{k},\omega)$, where $\underline{k}$ is the wavenumber vector and ω represents frequency. This continuous

transform is then discretized into finite sums following the work of Kraichnan (1970) and Drummond et al. (1984). Further assuming that a relatively narrow range of ω contributes at a particular $\underline{k}$ for the larger eddies, Fung et al. (1990) develop the representation of the sub-grid-scale flow field $\underline{u}'(\underline{x},t)$ in terms of N spectral components as

$$\underline{u}'(\underline{x},t) = \sum_{n=1}^{N} \{ [\, \underline{a}_n(t) \otimes \hat{k}_n \,] \cos \alpha_o(t) + [\underline{b}_n(t) \otimes \hat{k}_n \,] \sin \alpha_o(t) \} \tag{44}$$

where

$$\alpha_o(t) \equiv \underline{k}_n \circ \left[\underline{x} - \underline{x}_{on}(t) - \underline{u}t \right], \tag{45}$$

$\underline{u}$ is the mean flow,

$$\underline{x}_{on}(t) \equiv \underline{x}_{on}(t - \Delta t) + \underline{u}_{on}(t) \tag{46}$$

Δt represents a migrating spatial offset position of the nth spectral component,

and the vector amplitudes $\underline{a}_n(t)$, $\underline{b}_n(t)$

and eddy migration velocity $\underline{a}_{o_n}(t)$

each evolve according to a Langevin type equation with a relevant Lagrangian time scale,

$$T_n = 1/\omega_n = 1/(\sigma_{u'_n} \cdot k_n), \tag{47}$$

with $\sigma^2_{u'_n}$ representing the velocity variance of the nth spectral component. As the components of $\underline{u}'(\underline{x},t)$ are generated by vector cross products (that is, $\otimes$) of the $\underline{a}$, $\underline{b}$ amplitudes and the $\hat{k}_n$ unit vector, the divergence relation, $\nabla \circ \underline{u}' = 0$, is equivalent to the sum on n of the dot products, $\underline{k}_n \circ \underline{u}'_n$, is therefore immediately satisfied.

Equation (44) therefore contains nine randomly evolving quantities for each spectral component n. The fact that the sine and cosine pieces evolve independently implies that neither standing wave nor traveling wave (that is, $\exp[\pm\, i\alpha_o(t)]$) solutions are allowed to persist. The definition of the appropriate time scale, T_n, and the practical constraint that Langevin equations

should be marched at a time step, Δt, such that $\Delta t \ll T_n$, implies that the smallest eddies modeled (that is, largest k_n) will dictate the time step for advancing particle trajectories. Among other problems, excessively large time steps would imply that particles would not follow local streamlines and a principal feature of the divergence free flow aspect of the formulation (that is, avoidance of particle accumulation in zones of low turbulence) would be lost. This constraint on Δt suggests that the turbulent spectrum modeled by the KS approach be chopped off at a k value representing an appropriate trade off in realism and computational cost, and the effect of the high frequency remainder of the spectrum be included as a random walk or Langevin equation component of the particle's motion. Such an approach has recently been suggested in Sakai et al. (1991), by the Cambridge University team, responsible for many of the advances in KS theory, as a more economical alternative to their original approach (for example, Fung et al., 1990) involving separate but explicit treatment of the smaller "inertial" eddies that are carried along by the larger "sweeping" eddies considered here.

Fung et al. (1990) also provide guidance on developing vector amplitudes, $(\underline{a}_n, \underline{b}_n)$, the random component of the eddy migration velocity, $\underline{u}_{an}$, and choice of appropriate wave number values k_n. Each of the above 9N components of $\underline{a}$, $\underline{b}$, and $\underline{u}_a$ are chosen to have zero mean, a variance of $\sigma^{2'}_{u'_n}$, and an absence of covariance terms. Despite this lack of covariance in the vector amplitudes, turbulent velocity components will display appropriate negative normalized covariances of order - 1/2.

The equation (44) representation of the turbulent flow field is most appropriate for isotropic turbulence. In the case of anisotropic turbulence, the time scales, T_n, of equation (47) could easily be made vector quantities; however, due to the generation of velocity components via a cross product relation (for example, the x component of $\underline{u}'$ involves both the y and z components of the $\underline{a}$, $\underline{b}$ amplitudes), it becomes difficult to drive the independent Langevin equations for the amplitudes with an appropriate time scale. In addition, equation (44) is most appropriate for an unbounded medium (that is, no obstacles). The presence of a solid surface, such as the ground at z = 0 may be handled by the method of images or may be designed explicitly for that geometry, as will be done subsequently for a surface at z = 0. In the case of the surface at z = 0, the image method would suggest the combination

$$\underline{u}'_{odd} = [\underline{u}'(x,y,z,t) - \underline{u}'(x,y,-z,t)]/2 \qquad (48)$$

as that appropriate for ensuring that only those velocity components that are odd in z would survive. This procedure will, of course, kill off all threee components of the resultant $\underline{u}'_{odd}$ at z = 0, whereas it may be desired to eliminate only the z component of velocity at the surface.

The limitations of turbulence isotropy and suppression of the normal component (w') at a z = 0 surface that are embedded within equation (48) may be eliminated by developing a customized set of equations for the turbulent velocity components. One such possibility, for the nth spectral component, is given as

$$w' = [a_3 \cos \alpha_3 + b_3 \sin \alpha_3] \sin(k_z \cdot z) \tag{49}$$

$$u' = (k_z/kx)\ [-a_3\beta^2 \sin \alpha_3 + b_3\ \gamma^2 \cos \alpha_3]_{\cos}\ (k_z \cdot z) + (k_y/k_t)\ [a_t \sin \alpha_1 \cos \alpha_2\ b_T \cos \alpha_1 \sin \alpha_2] \tag{50}$$

$$v' = (k_z/k_y)\ [-a_3(1-\beta^2) \sin \alpha_3 + b_3\ (1-\gamma^2) \cos \alpha_3] \cos\ (k_z \cdot z) + (k_x/k_T)\ [-a_T \cos \alpha_1 \sin \alpha_2 - b_T \sin \alpha_1 \cos \alpha_2] \tag{51}$$

where

$\alpha_1 = k_y(y - y_{o1} - vt) + k_z(z - z_{o1} - wt)$,

$\alpha_2 = k_x(x - x_{o2} - ut) + k_z(z - z_{o2} - wt)$,

$\alpha_3 = k_x(x - x_{o3} - ut) + k_y(y - y_{o3} - vt)$,

$k_T = (k_x^2 + k_y^2)^{\frac{1}{2}}$, and

the four a, b amplitudes, the six coordinates (x_{o2}, x_{o3}, y_{o1}, y_{o3}, z_{o1}, z_{o2}) and the two projection operators β, γ are all allowed to evolve in time via separate Langevin equations. It should also be noted that the nearly ubiquitous subscript n has been dropped.

In the above equations, the (a_3, b_3) amplitudes determine the strengths of two-dimensional eddies lying in the x-z and y-z planes with the projection operators (β,γ) defined such that $-1 \leq \beta, \gamma \leq +1$, determine the apportionment between x and y fractions. Similarly the (a_T, b_T) amplitudes determine the strengths of two-dimensional eddies and convergence/divergence zones in the x-y plane.

A principal advantage of the equation (49) formulation is that the time scales, T_3, which govern the evolution of the vertically oriented eddies can be completely decoupled from the time scales, T_T, of the longer lived transverse fluctuations in the x-y plane given by equations (50) and (51). We also note that the simple z dependence, $\sin(k_z \cdot z)$, could easily be generalized to a more general form, f(z), with the additional requirement being that the $\cos(k_z \cdot z)$ dependence in u', v' be replaced with df(z)/dz. Additional z dependence may also be added to the transverse eddy components as needed to provide more realistic vertical profiles of turbulent velocity moments.

3. MULTI-SPECTRAL SMOKE ASPECTS OF THE PROBLEM

3.1 Dry Deposition of Particles

Many complex processes are involved in the transfer and deposition of pollutants at the surface. Sehmel (1980) compiled a list of the factors known to influence dry deposition rates (see table 1). The variables listed include the properties of the depositing material (for example, particle size and density; gas diffusivity, solubility, and reactivity), the characteristics of the surface (for example, surface roughness, vegetation type, amount, and physiological state),

and atmospheric variables (for example, stability, turbulence intensity). Hicks (1982) noted the important differences controlling the deposition of larger particles (for example, gravitational settling, inertial impaction) and those controlling gases (for example, turbulence, molecular diffusion). Deposition of small particles is complicated by the fact that they may be influenced by the processes affecting both gases and large particles. Figure 3 shows the tremendous variability of deposition velocity to particle size alone.

TABLE 1. FACTORS INFLUENCING DRY DEPOSITION RATES*

Micrometeorological Variables	Depositing Material	Surface Variables
Aerodynamic roughness	Particles	Accommodation
- Mass transfer		- Exudares
(a) Particles	Agglomeration	- Trichomes
(b) Gases	Diameter	- Pubescence
- Heat	Density	- Wax
- Momentum	Diffusion	Biotic surfaces
Atmospheric stability	- Brownian	Canopy growth:
Diffusion, effect of:	- Eddy equal to	- Dormant
- Canopy	(a) Particle	- Expanding
- Diurnal variation	(b) Momentum	Senescent
- Fetch	(c) Heat	Canopy structure:
Flow separation:	- Effect of canopy on	- Areal density
- Above canopy	Diffusiophoresis	- Bark
- Below canopy	Electrostatic effects	- Bole
Friction velocity	- Attraction	- Leaves
Inversion layer	- Repulsion	- Porosity
Pollutant concentration	Gravitational settling	- Reproductive structure
Relative humidity	Hygroscopicity	- Soils
Seasonal variation	Impaction	- Stem
Solar radiation	Momentum	- Type
Surface heating	Physical properties	Electrostatic properties
Temperature	Resuspension	Leaf-Vegetation:
Terrain	Shape	- Boundary layer
- Uniform	Size	- Change at high winds
- Nonuniform	Solubility	- Flutter
Turbulence	Thermophoresis	- Stomatal resistance
Wind velocity		Non-biotic surfaces
Zero-plane displacements	Gases	pH effects on:
- Mass transfer		- Reaction
(a) Particles	Chemical activity	- Solubility
(b) Gases	Diffusion:	Pollutant penetration and distribution in canopy
- Heat	- Brownian	Prior deposition loading
- Momentum	- Eddy	Water
	Partial pressure in equilibrium with surface	
	Solubility	

*from Sehmel, 1980

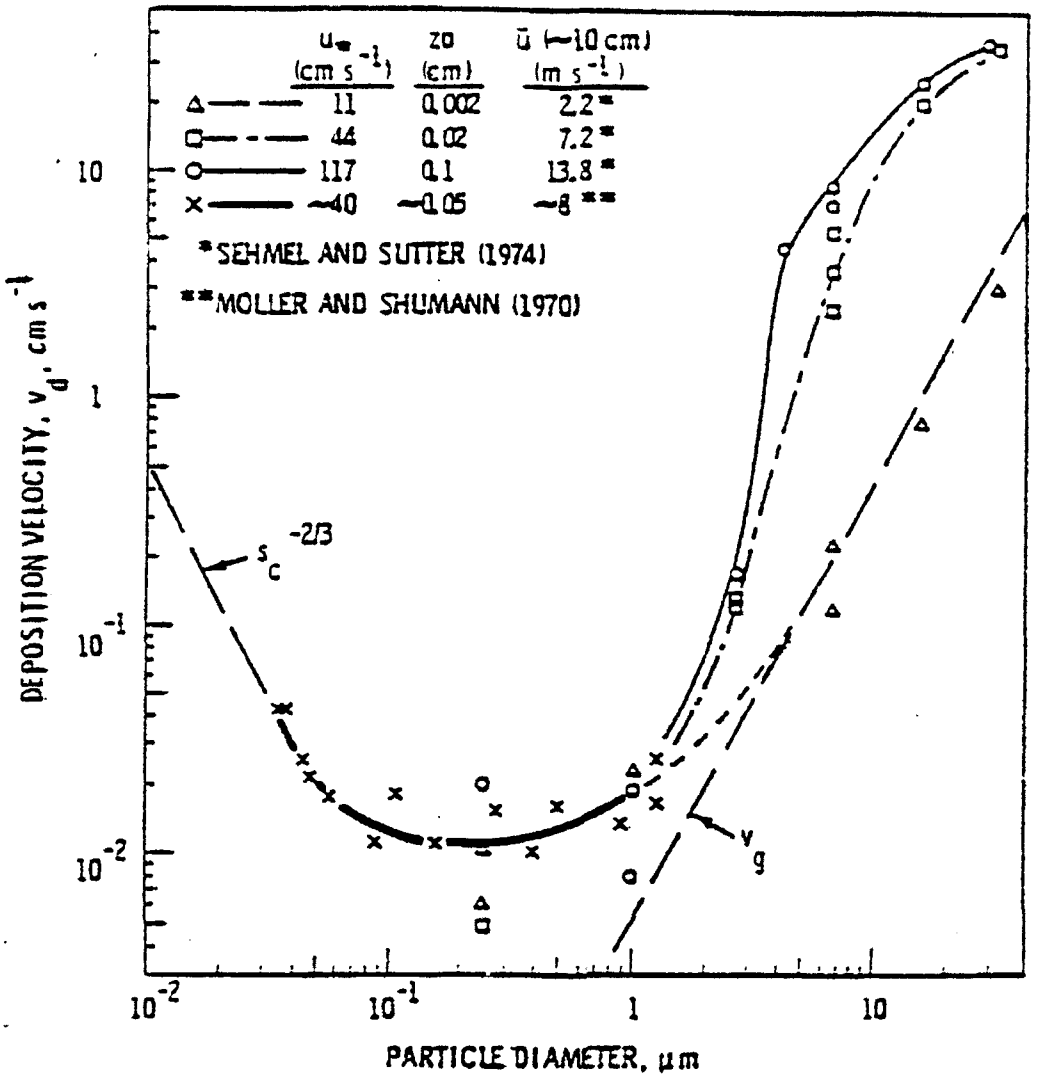

Figure 3. Observed deposition velocities as a function of particle size for 1.5 g/cm^3 density particles. Measured by Sehmel and Sutter (1974) and Moller and Schumann (1970). Figure from Slinn et al. (1978).

Although it is not practical, or even understood how, to include all of the variables listed in table 1 into the deposition model, it is possible to parameterize many of the most important effects known to control deposition rates, using only directly-available or easily-computed variables which describe the state of the atmosphere, surface conditions, and pollutant properties.

Many models of dry deposition express the deposition velocity as the inverse of a sum of "resistances" plus, for particles, gravitational settling velocity terms. The resistances represent the opposition to transport of the depositing material from a reference height through the turbulent atmospheric surface layer, and through a quasi-laminar layer just above the surface to the surface itself. The major processes that determine these resistances are briefly described below.

3.1.1 Gravitational settling

The gravitational settling velocity is a function of the particle size, shape, and density. Figure 4 shows the gravitational settling velocity (V_T in the figure) as a function of particle size for several values of the particle

density. Note that the gravitational settling velocity represents a lower limit to the deposition velocity. It can be seen that for larger particles, in the range of 20 to 40 μm in diameter and higher, the deposition velocity approaches the settling velocity, which indicates that the rate of deposition is dominated by the gravitational settling mechanism. The gravitational settling velocity decreases with decreasing particle size and density. However, for particles smaller than about 20 μm in diameter, the deposition velocity curve shows larger and larger deviations from the gravitational settling curve as the particle size decreases. This is due to the effect of other mechanisms, discussed below, in enhancing the deposition rates of smaller particles above those predicted by gravitational settling alone.

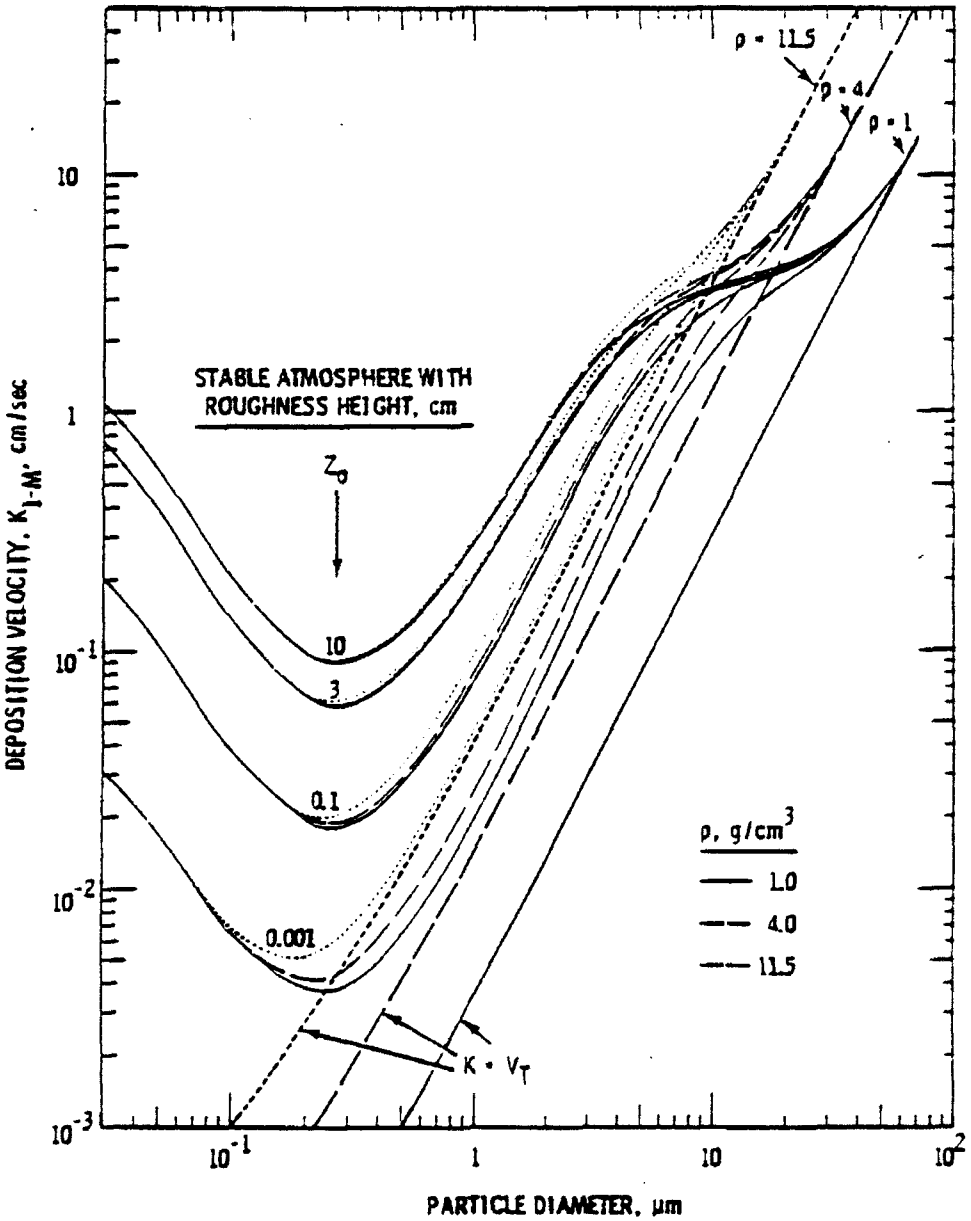

Figure 4. Predicted deposition velocities for $u_* = 100$ cm/s and particle densities of 1, 4, and 11.5 g/cm^3. Also shown is the gravitational settling velocity (V_T). Figure from Sehmel (1980).

3.1.2 Atmospheric diffusion

The rate of deposition can sometimes be limited by the transfer of pollutant material to the vicinity of the surface by atmospheric turbulence. For example, this would typically occur during very stable conditions for an elevated plume of material composed of small-sized particles with small gravitational settling velocities. In the lowest layer of the atmosphere, the aerodynamic resistance is used to parameterize the rate of mixing in terms of the windspeed, atmospheric stability, and surface roughness length. The aerodynamic resistance generally decreases (that is, the deposition velocity will increase) with increasing windspeed and/or surface roughness.

3.1.3 Quasi-laminar layer.

Over smooth surfaces, a thin nonturbulent sublayer develops that can be a significant obstacle to the transfer of the pollutant onto the surface. For rough, real-world surfaces, this sublayer is constantly changing and is likely to be intermittently turbulent. For this reason, Hicks (1982) calls this layer the "quasi-laminar" layer. It is also know as the deposition layer. Small particles (< 0.05 μm in diameter) are transported through the quasi-laminar layer primarily by Brownian diffusion. This process becomes less efficient as the particle size increases. Particles in the 2- to 20-μm diameter range tend to penetrate the quasi-laminar layer by inertial impaction. However, particles larger than 20 μm in diameter are less efficiently captured, so the inertial impaction mechanism is most effective in the 2- to 20-μm diameter size range. Because particles in the 0.1- to 1.0-μm diameter size range are not efficiently transported across the quasi-laminar layer by either Brownian diffusion or inertial impaction, particles in this size range have the lowest deposition velocities.

Several candidate deposition models that parameterize some or all of the physical processes described above have been selected for further study. Individual components of other models have also been reviewed. Ultimately, it may be advantageous to combine the best features of several algorithms into a hybrid model. Brief descriptions of the various models for computing deposition velocities of particulate matter are provided below. The data requirements of all the models considered are relatively simple (particle size, density, surface roughness, and routine meteorological parameters to compute the friction velocity and Monin-Obukhov length). Some initial results of sensitivity testing and intercomparisons of the models are also summarized below.

3.1.3.1 Sehmel model. Sehmel (1980) and Sehmel and Hodgson (1978) proposed a model for predicting deposition velocities of particles above smooth surfaces. The basis of the model is a set of wind tunnel observations of deposition for monodispersed particles to surfaces such as gravel, artificial grass, brass shim stock, and water. The model consists of empirical equations for transfer resistances derived from a least-squared empirical fit of deposition velocity as a function of particle size, density, surface roughness, and friction velocity. The equations were converted into a computer code by B. Croes of the California Air Resources Board (CARB) and is sometimes known as the CARB model. It is also used in the fugitive dust model (FDM).

In the Sehmel approach, integrated resistances to mass transfer are computed within two layers. The first layer extends from a reference height of 1 m down to 1 cm above the surface. In this layer, atmospheric turbulence dominates mass transfer. Eddy diffusivities are used to describe the transfer rate. The second layer is the deposition surface layer within one centimeter of the surface. The integrated resistance within the deposition surface layer is derived from a statistical fit of the wind tunnel particle deposition data. Sehmel and Hodgson express the deposition velocity as:

$$v_d = \frac{v_g}{1. - \exp[-v_g(I_{12} + I_3)/u_*]} \tag{52}$$

where

v_d is the deposition velocity (cm/s),

v_g is the gravitational settling velocity (cm/s),

I_{12} is the atmospheric diffusional resistance (dimensionless),

I_3 is the surface resistance integral (dimensionless), and,

u_* is the surface friction velocity.

The atmospheric diffusion resistance used by Sehmel and Hodgson (1978) is based on the flux profile relationships of Businger et al. (1971). For neutral or stable conditions,

$$I_{12} = (\ln(z_1/z_2) + 4.7(z_1 - z_2)/L)/k \tag{53}$$

where

z_1 is the upper limit of the atmospheric diffusional resistance integral (that is, 100 cm),

z_2 is the lower limit of integral (that is, 1 cm),

L is the Monin-Obukhov length (cm), and,

k is the von Karman constant (Sehmel used a value of 0.35).

For unstable conditions, the atmospheric diffusional resistance integration yields:

$$I_{12} = (\ln\{|(A_{z1} - 1.)(A_{z2} + 1.)|/|(A_{z1} + 1.)|\} + 2.[\tan^{-1}(A_{z1}) - \tan^{-1}(A_{z2})]/k \tag{54}$$

$$A_{z1} = (1. - 15.z_1/L)^{0.25} \tag{55}$$

$$A_{z2} = (1. - 15.z_2/L)^{0.25} \tag{56}$$

The surface resistance integral is an empirical relationship based on wind tunnel observations. For particles with a diameter > 0.01 mm,

$$I = exp\ \{-378.051 + 16.498\ln(Sc) + \ln(t)\ [\ -11.818 - 0.2863\ \ln(t\ ) + 0.3226\ln(d\ 10\ /z\ ) - 0.3385\ \ln(D/z\ u\ ))] - 12,804\ln(d\ 10\ )\} \quad (57)$$

where,

D is the Brownian diffusion coefficient (cm /s),

t is a relaxation time (dimensionless),

Sc is the Schmidt number,

z is the surface roughness length (cm), and,

d is the particle diameter (mm).

Sehmel's formulation generally shows a reasonable variation of deposition velocity as a function of its model parameters (that is, density, size, surface roughness, friction velocity). The predicted deposition velocity is close to the gravitational settling velocity for large particles (for example, greater than about 20 mm diameter), and decreases with decreasing particle size to about 0.1 mm to 1.0 mm, where it reached a minimum. The deposition velocity then increases with decreasing particle size for smaller sized particles. This behavior is consistent with the importance of Brownian motion in enhancing deposition rates for very small particles. The Sehmel scheme produces increased deposition rates for increased particle density, surface roughness lengths, and friction velocities. Recent laboratory studies by Noll and Fang (1989) suggest, however, that Sehmel's model may underpredict deposition velocities fo particle diameters greater than about 30 mm.

A main limitation of the scheme stems from the lack of generality of the highly empirical relationship for the surface resistance integral (equation (57)). I is based on wind tunnel data for relatively smooth surfaces under a limited range of conditions. For example, in order to avoid extrapolation, the CARB implementation of the model does not allow the surface roughness length used in the algorithm to exceed 10 cm, even though many real world surfaces have significantly greater roughness lengths. In addition, sensitivity testing of the model has shown that it exhibits some nonphysical behavior when the inputs are varied beyond the range of conditions tested in the wind tunnel. For example, the Sehmel model shows a very strong sensitivity to temperature which is not exhibited by other deposition models. For particles in the 0.1- to 1.0-μm diameter size, a change of nearly an order of magnitude in deposition velocity was predicted for a temperature change from 0 °F to 100 °F (figure 5). This nonphysical behavior is probably an artifact of the regression equations used to fit the surface resistance integral to the wind tunnel data. The original wind tunnel tests were performed at a constant temperature, and, as a result, application to a realistic range of atmospheric conditions involves extrapolation outside the range on which the model was developed.

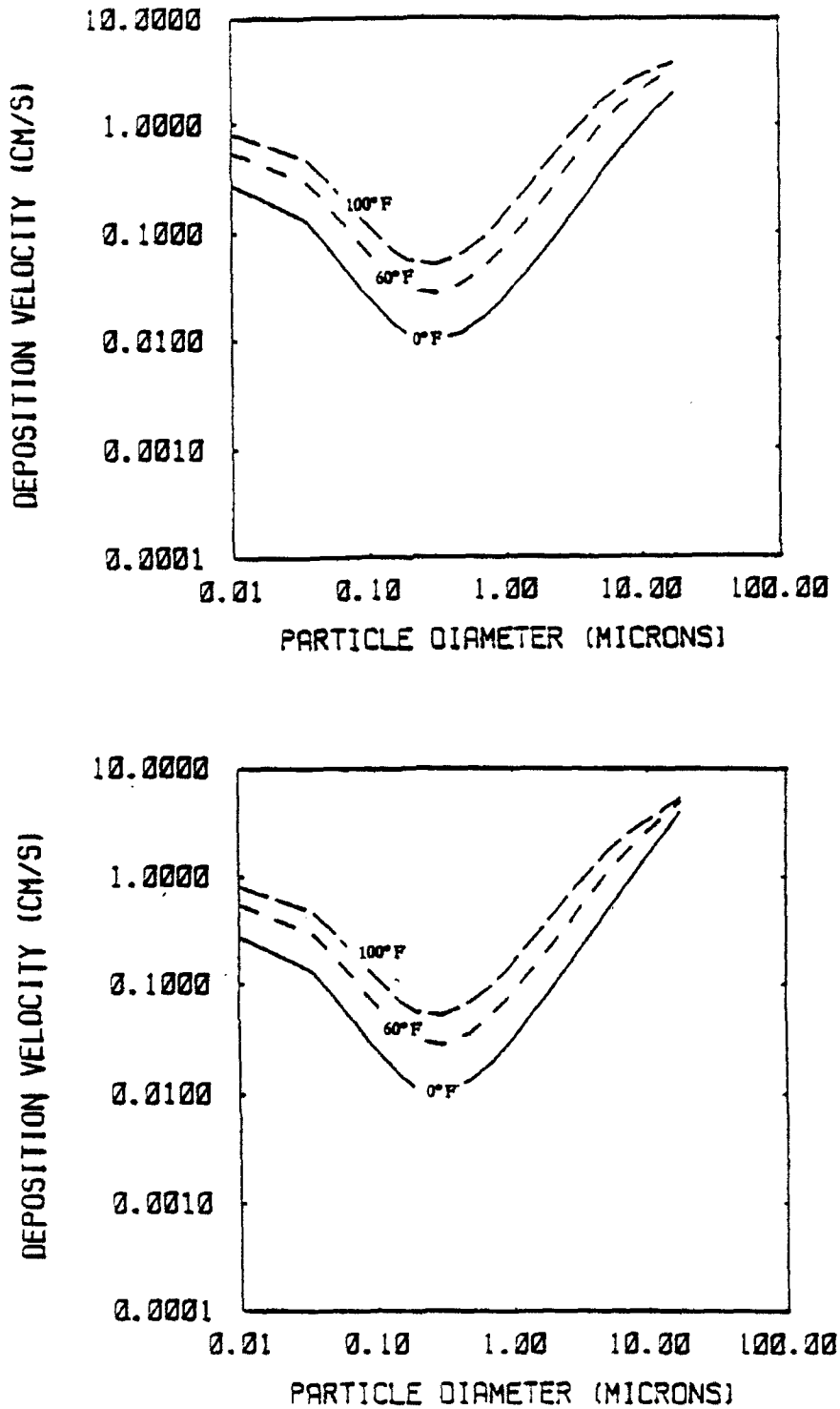

Figure 5. Deposition velocity as a function of particle diameter as predicted by the Sehmel/CARB model for three different values of ambient temperature (0°, 60°, 100 °F) and densities of 1 g/cc (top) and 4 g/cc (bottom). The assumed neutral flow has a $u_* = 0.5$ m/s over a surface of $z_o = 0.1$ m.

A second problem noted from the sensitivity testing is that the deposition velocity curves display a kink at a particle diameter of about 0.03 μm. For particles smaller than about 0.1 μm in diameter, the deposition velocity increases with decreasing particle diameter. However, the Sehmel model shows this trend only to about 0.03 μm in diameter, beyond which the deposition velocity is predicted to decrease or level off with decreasing particle diameter (see figure 6). These kinks in the deposition velocity curves appear to be another artifact of use of the regression equations outside the range of conditions on which the model was developed. These limitations have some implications on the ability of this model to handle the entire range of likely applications.

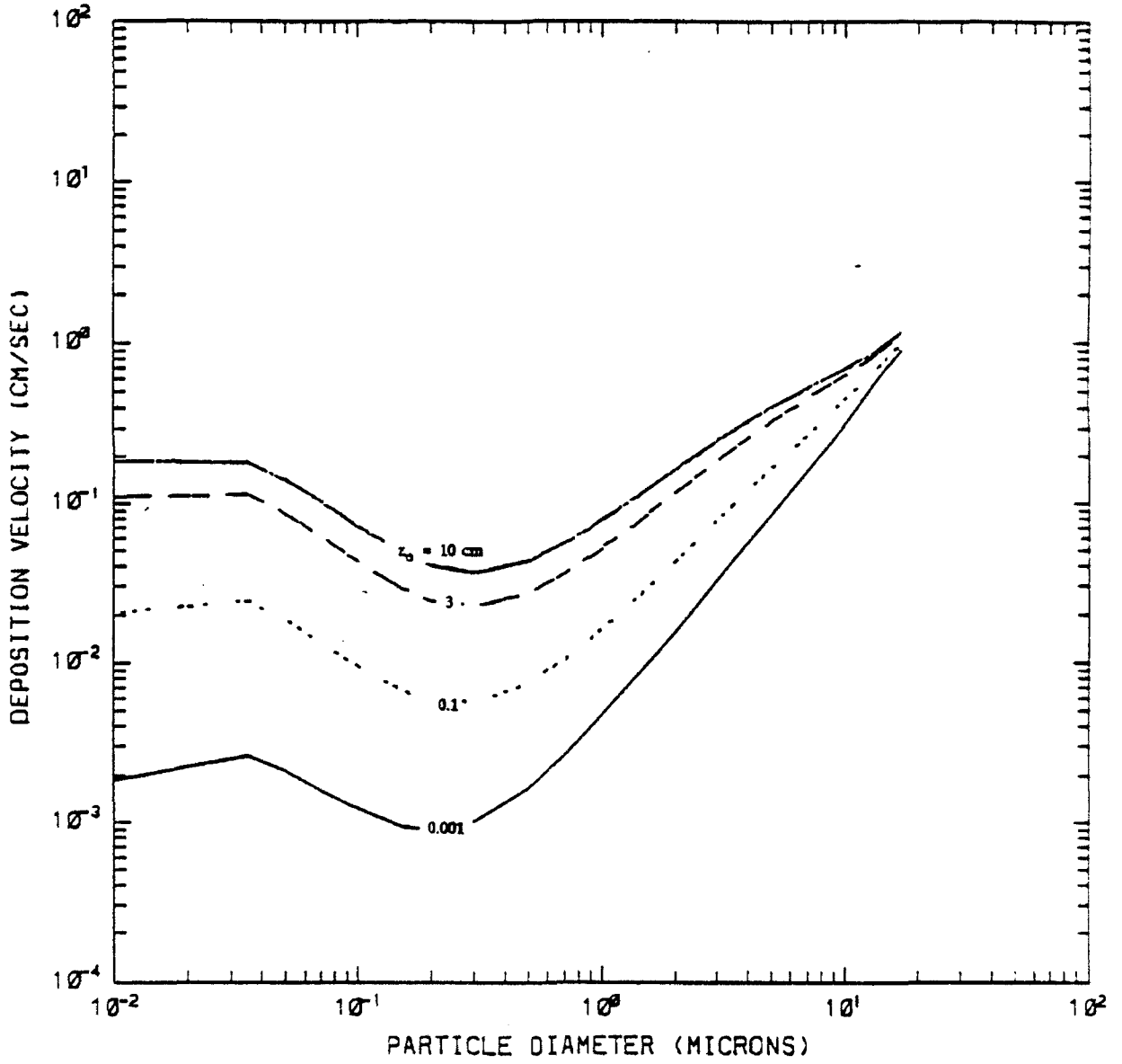

Figure 6. Deposition velocity as a function of particle diameter as predicted by the Sehmel/CARB model for surface roughness lengths of 0.001, 0.01, 3, and 10 cm. The particles have an assumed density of 1 g/cc and are in a neutral flow with u* = 0.1 m/s.

3.1.3.2 **Resistance models.** Resistance-based models for particle deposition have been used in many models, including ADOM (Pleim et al., 1984), CALPUFF (Scire et al., 1990), CALGRID (Yamartino et al., 1989), and a new version of the Urban Airshed Model, UAM-V. The basic approach used in these models is similar, with special enhancements or features designed to accommodate the specific focus of the model (for example, oxidants, secondary particulate matter, toxic pollutants). Although some of these models are mesoscale or regional scale Eulerian grid models (for example, ADOM, CALGRID), their deposition formulations are suitable for application to Gaussian plume or Lagrangian particle models on much smaller horizontal spatial scales.

The general approach used in the resistance models is to include explicit parameterizations of the effects of Brownian motion, inertial impaction, and gravitational settling. The deposition velocity is written as the inverse of a sum of resistances to pollutant transfer through the atmosphere to the surface, plus gravitational settling terms (Slinn and Slinn, 1980; Pleim et al., 1984).

$$v_d = \frac{1}{r_a + r_d + r_a r_d v_g} + v_g \qquad (58)$$

where

v_d is the deposition velocity (cm/s),

v_g is the gravitational settling velocity (cm/s),

v_a is the aerodynamic resistance (s/cm), and

v_d is the deposition layer resistance (s/cm).

Note that for large settling velocities, the deposition velocity approaches the settling velocity ($v_d \rightarrow L\ v_g$), whereas, for small settling velocities, v_d tends to be dominated by the r_a and r_d resistance terms.

The lowest few meters of the atmosphere can be divided into two layers -- a fully turbulent region where vertical fluxes are nearly constant, and the thin quasi-laminar sublayer. The resistance to transport through the turbulent, constant flux layer is referred to as the aerodynamic resistance. It is usually assumed that the eddy diffusivity for mass transfer within this layer is similar to that for heat. The atmospheric resistance formulation used in all of the resistance models is based on Wesely and Hicks (1977).

$$r_a = \frac{1}{k\ u_*} [ln\ (z/z_o) - \psi_H] \qquad (59)$$

where

Ψ_H is a stability adjustment factor,

u_* is the surface friction velocity,

k is the von Karman constant (0.4),

z is height (m), and

z_o is the surface roughness length (m).

The parameterization of the deposition layer resistance terms varies somewhat. The approach used by Pleim et al. (1984) is:

$$r_d = \left[Sc^{-2/3} + 10^{-3/St} \right]^{-1} u_*^{-1} \qquad (60)$$

where

Sc is the Schmidt number ($Sc = \nu/D$),

ν is the viscosity of air,

D is the Brownian diffusivity of the pollutant in air,

St is the Stokes number [$St = (v_g/g)(u_*^2/\nu)$], and

g is the acceleration due to gravity (9.8 m/s^2).

The first term of equation (60), involving the Schmidt number, parameterizes the effects of Brownian motion. This term controls the deposition rate for small particles. The second term, involving the Stokes number, is a measure of the importance of inertial impaction. The inertial impaction term tends to dominate for intermediate-sized particles in the 2- to 20-μm diameter size range.

The deposition formulation in UAM-V is still under development, and is currently being reviewed by Sigma Research under the Lake Michigan Oxidant Study (LMOS) program. Its main difference from that of Pleim et al. (1984) lies in the formulation of the inertial impaction term of r_d. That is,

$$r_d = \left[C_1 Sc^{-2/3} + C_2 St \right]^{-1} u_*^{-1} \qquad (61)$$

where C_1, C_2 are constants, linearizes the appearance of the Stokes number.

These models produce a pattern of deposition velocity as a function of particle size and density, similar to that of Sehmel. However, the ADOM/CALPUFF/ CALGRID approach of Pleim et al., tends to predict somewhat higher deposition velocities in the 5- to 15-μm diameter size range than the Sehmel model and lower values in the 0.1 to 5.0-μm diameter range. Although the general shape of the deposition velocity curves are similar, the minimum deposition velocity in the Pleim et al. formulation tends to occur at larger particle diameters (that is, closer to 1.0 μm than 0.1 μm) than in the Sehmel model. The constants C_1 and C_2 in the UAM-V scheme were derived to force a minimum deposition velocity at 0.2 μm diameter.

The parameterizations of the resistance models for Brownian motion and inertial impaction effects involve empirical factors derived from a number of field and wind tunnel studies. The sensitivity analyses with these models shows no unusual response to temperature variations over the ambient temperature range from 0 °F to 100 °F. These resistance models also all show a steady increase of deposition velocity with decreasing particle diameter in the small particle range (< 0.1 μm in diameter).

Figures 7 thru 10 display predictions of the UAM deposition velocity model for particle sizes ranging from 10^{-2} μm to 20 μm and for seven different values of surface roughness, z_o, ranging from 10^{-3} cm to 100 cm. Figures 7 and 8 are for stable meteorological conditions with friction velocity values of 0.1 m/s and 0.5 m/s, respectively, whereas figures 9 and 10 involve the assumption of convective conditions. As most of the deposition variability is due to u_*, the influences of surface roughness and stability per se are seen to be relatively small.

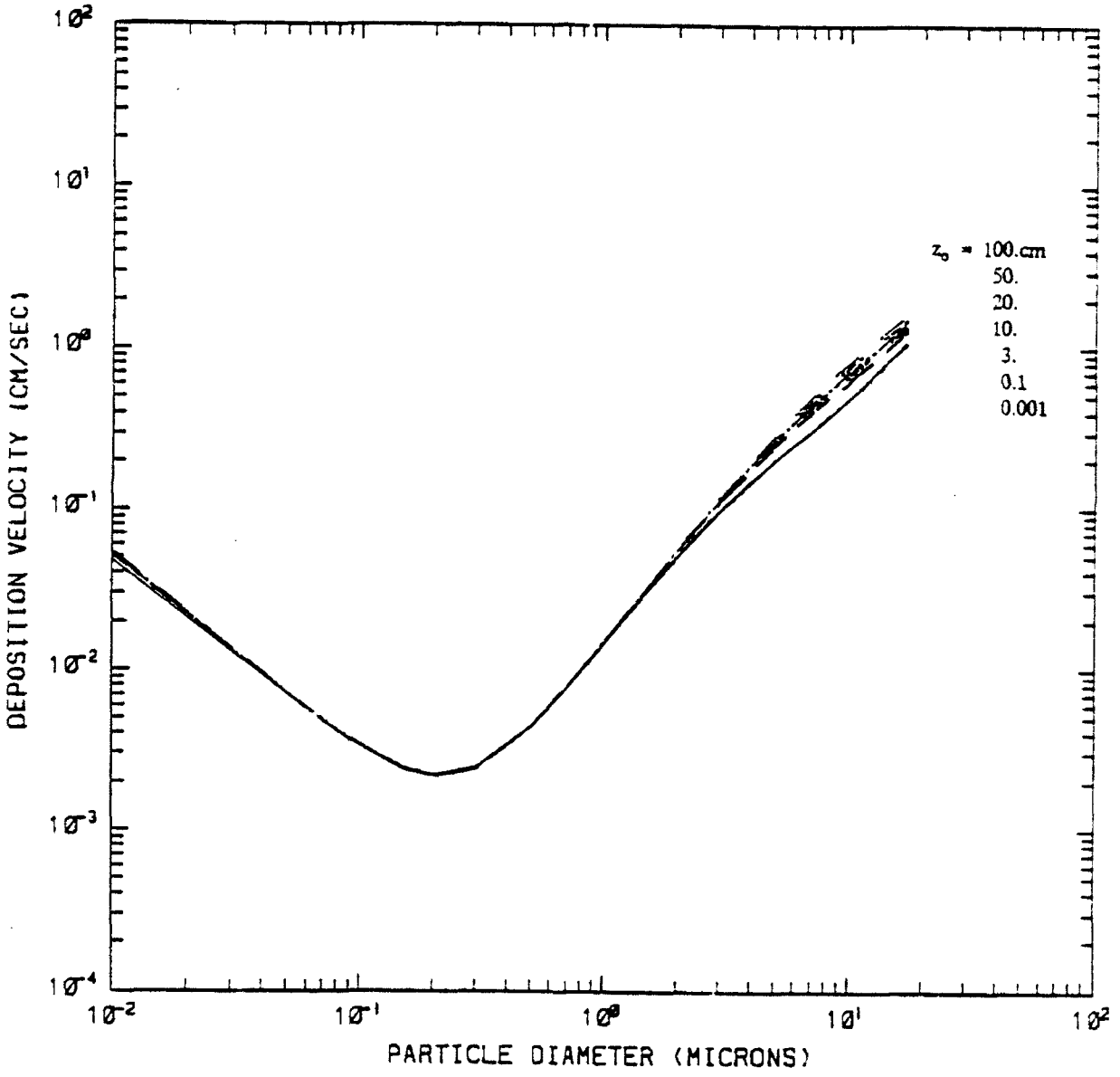

Figure 7. Deposition velocity versus particle size as predicted by the UAM-V model for surface roughnesses of 10^{-3}, 10^{-1}, 3, 10, 20, 50, and 100 cm. The model predicted deposition velocities are for particles with a density of 1 g/cc in a flow with stable stratification and a friction velocity of 0.1 m/s.

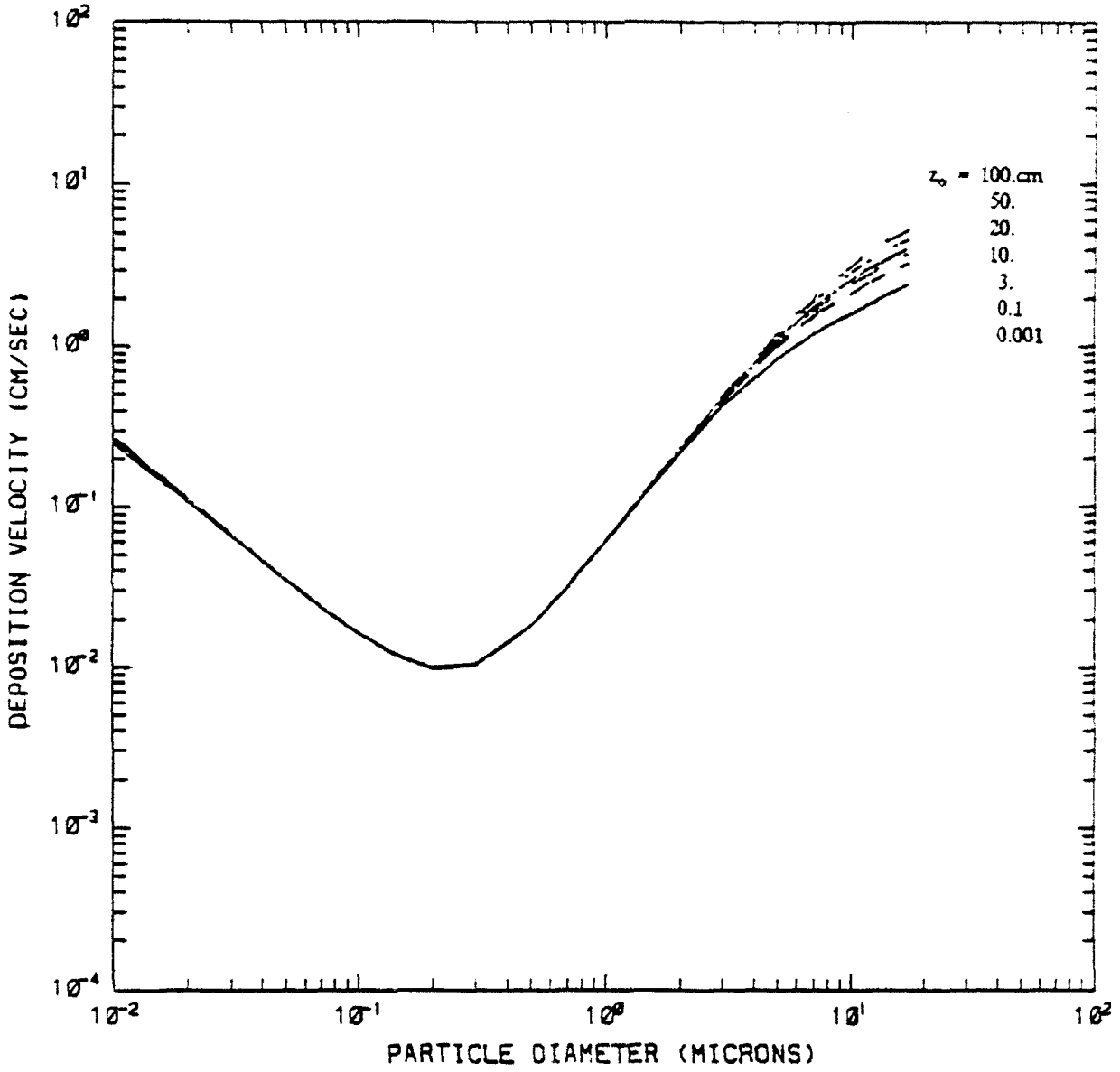

Figure 8. Deposition velocity versus particle size as predicted by the UAM-V model for surface roughnesses of 10^{-3}, 10^{-1}, 3, 10, 20, 50, and 100 cm. The model predicted deposition velocities are for particles with a density of 1 g/cc in a flow with stable stratification and a friction velocity of 0.5 m/s.

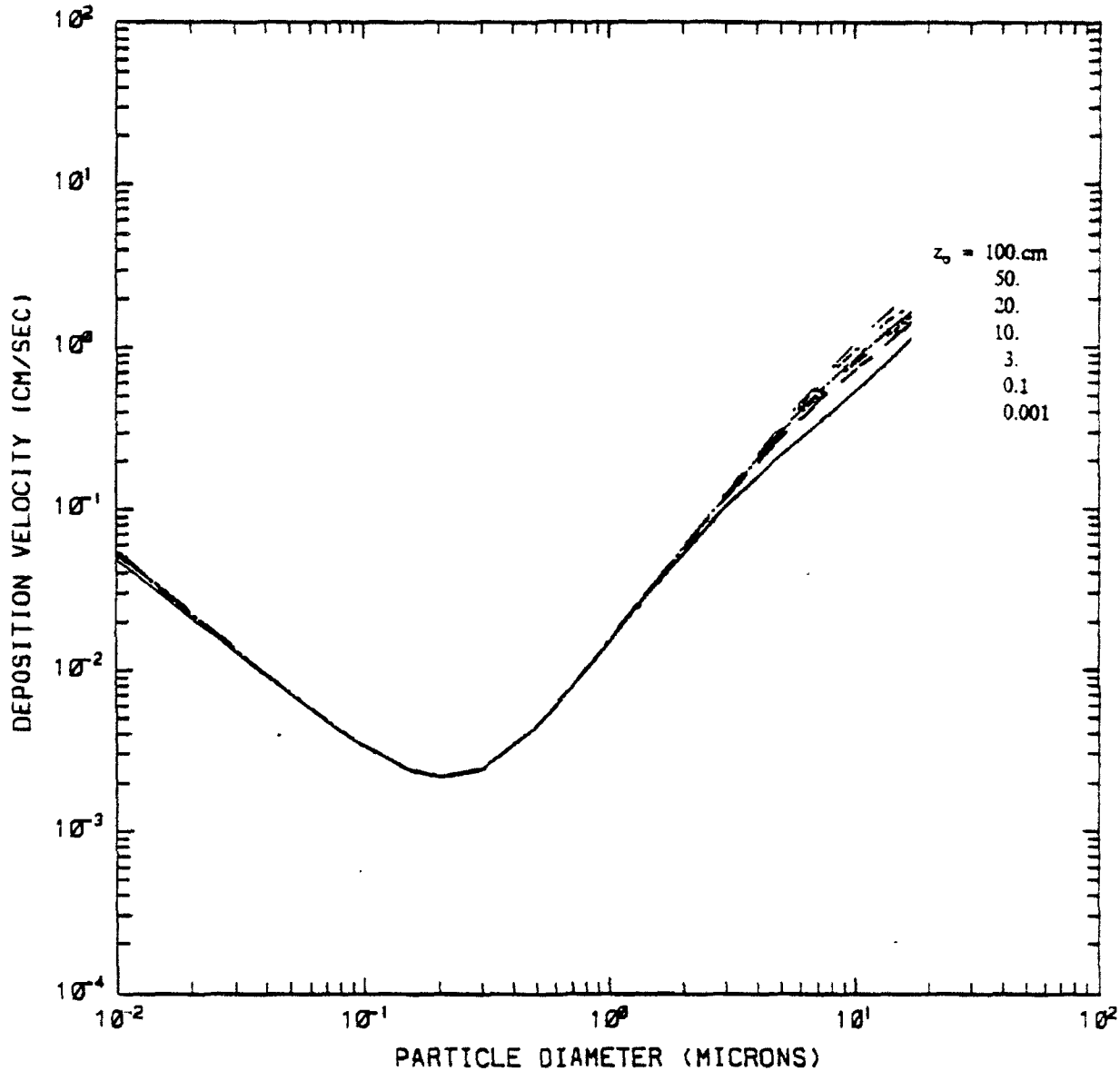

Figure 9. Deposition velocity versus particle size as predicted by the UAM-V model for surface roughnesses of 10^{-3}, 10^{-1}, 3, 10, 20, 50, and 100 cm. The model predicted deposition velocities are for particles with a density of 1 g/cc in a flow with unstable stratification and a friction velocity of 0.1 m/s.

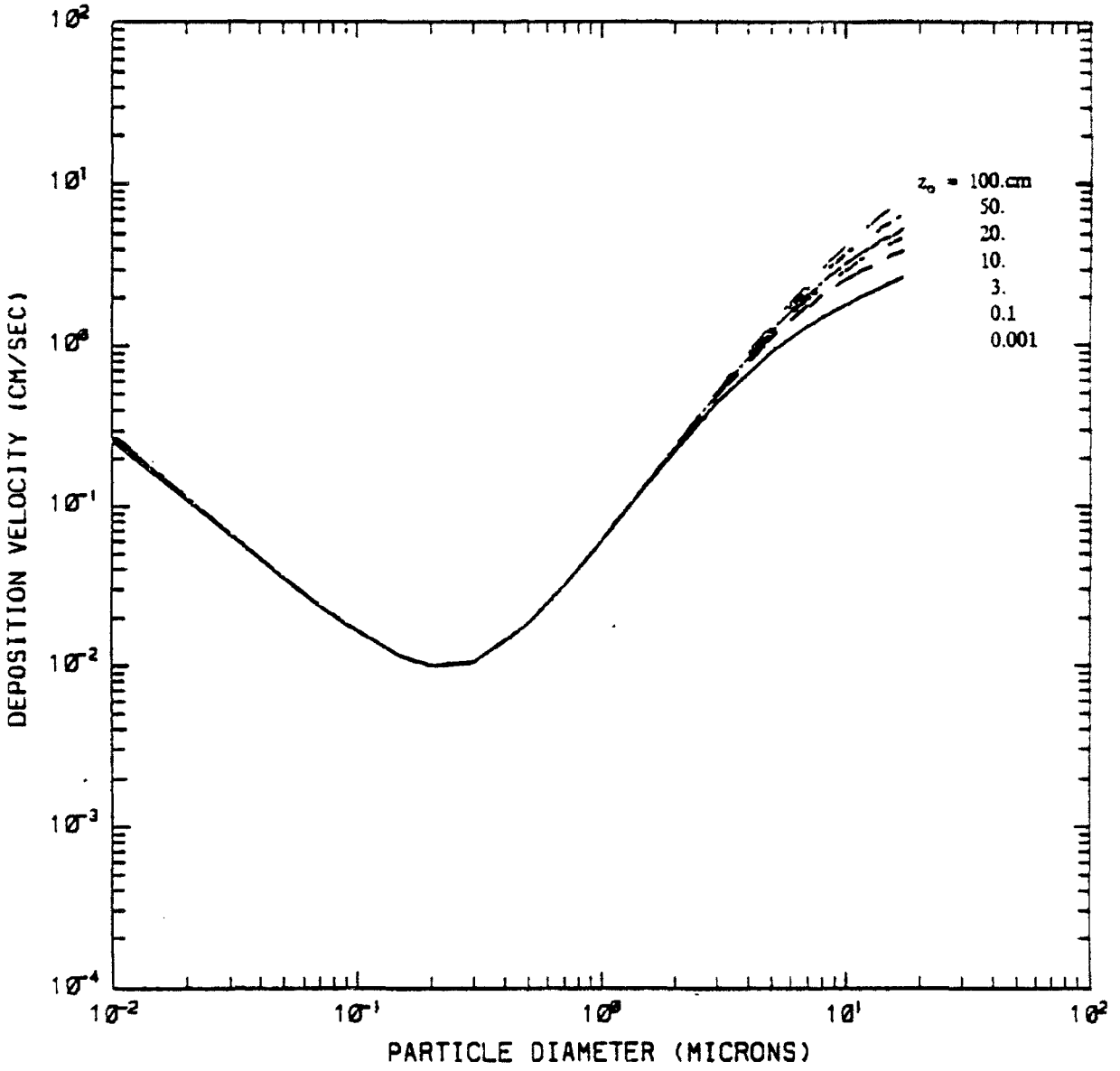

Figure 10. Deposition velocity versus particle size as predicted by the UAM-V model for surface roughnesses of 10^{-3}, 10^{-1}, 3, 10, 20, 50, and 100 cm. The model predicted deposition velocities are for particles with a density of 1 g/cc in a flow with unstable stratification and a friction velocity of 0.5 m/s.

3.2 Deposition Removal in Particle Models

There are two widely used methodologies for including dry deposition of particles--discrete particle removal and probabilistic reduction of particle mass. Both methods involve the computation of capture probabilities for the surface to ensure that the deposition flux, F, matches that predicted by the relation, $F = v_d \cdot C(z_{ref})$ where $C(z_{ref})$ is the concentration at the same reference height used in the computation of the deposition velocity, v_d.

In the case of discrete particle removal, particles with a trajectory time step end point below the surface, that is, $z_e < 0$ are either reflected, by reassigning this coordinate as $-z_e$, or absorbed to provide an appropriate deposition flux. Overcamp (1976) introduced a partial reflection formulation for Gaussian plume models including both dry deposition and gravitational settling, while Rao (1981) has developed a formulation based on an analytic solution of the equivalent gradient transfer theory problem. Janicke (1985) has extended the notion of partial reflection to Lagrangian particle models but has recently concluded (Janicke, 1990) that the notion of applying weights of zero or one to particle survival probabilities serves to increase the statistical uncertainty associated with counting particles (that is, counting statistics errors) for evaluating concentrations. In his LASAT-C model (Janicke, 1990), all particles which reach the $z = 0$ surface are reflected and a fractional survival probability, p_s, ($0 \leq p_s \leq 1$) is applied to all such particles. The probabilities so determined involve several velocity, time, and distance scales and the formalism is not obviously transferable to the envisioned KS turbulence formulation. In addition, such a scheme may continue to distribute capture probabilities across relatively few particles with higher attendant computational noise.

Zannetti and Al-Madani (1983) proposed a probabilistic method which also is applied only to those particles which have passed below the $z = 0$ surface. In their model, the fraction of particles which are deposited is specified as p_d, where

$$P_d = 1 - \exp(-\Delta t / T_d) \tag{62}$$

and T_d is the deposition time scale which is a function of all the variables influencing deposition. An analogous method is also developed to describe particle resuspension. Such a method is interesting both because it treats deposition as an exponential process and because it can be implemented either in discrete particle removal schemes or in mass reduction schemes. In probabilisti mass reduction schemes, the particle is not removed but instead assigned a reduced mass,

$$M(t + \Delta t) = (1 - p_d) \cdot M(t) \ , \tag{63}$$

for use in subsequent concentration calculations. This representation is more explicit in indicating that the fractional mass, p_s, (or probability of) surviving the deposition process is simply:

$$p_s = 1 - p_d = \exp(-\Delta t / T_d) \ , \tag{64}$$

and therefore treatable as an exponential process.

Equation (64) is also the form used to describe the surviving fraction of material in one-layer, long range transport models or in the lowest layer of multi-layer grid models and results directly from the solution of the first-order differential equation for material loss:

$$V \frac{dC}{dt} = -F \cdot A \tag{65}$$

where

V is the volume of the cell,

A is the cell's area in the x - y plane,

and

F is the deposition flux given as

$F = v_d \bullet C$ in terms of the deposition velocity v_d.

This differential equation is easily solved to yield,

$$p_s = C(\Delta t)/C(0) = \exp(-v_d \cdot \Delta t/H) \ , \tag{66}$$

where Δt is the duration of the time step, and $H = V/A$ is the cell's vertical depth over which the pollutant is assumed well mixed.

Equation (66) raises the interesting question of why should an arbitrarily defined cell depth H affect the deposition of material? In fact, it is easy to show that provided the cell is not excessively depleted (that is, $v_d \Delta t/H \ll 1$) the number of particles deposited, n_d, from a cell containing n_T total particles is just

$$n_d = n_t \cdot (v_d \cdot \Delta t/H) \ ; \tag{67}$$

however, the number of particles in the cell equals the number density concentration, C/m , (where m_o is mass per particle) times the cell volume, AWH, to yield

$$n_d = (C/m_o) \cdot A \cdot v_d \cdot \Delta t = (F/m_o) \cdot A \cdot \Delta t \tag{68}$$

thus, equation (68) shows that for $\phi = v_d \cdot \Delta T/H$ small enough that $1-\exp(-\phi) = \phi$ the depth of the cell is not of importance.

We now extend this concept to develop a model for particle survival probability that is a reasonable function of height, z, above the surface. The simplest such model that preserves the cumulative exponential nature of the process is

$$p_s(z) = A \cdot \exp(-\beta \ v_d \cdot \Delta t/z) \ , \tag{69}$$

where A is an overall normalization of order unity and β is a constant coefficient. The primary constraint that equation (69) must satisfy is that its average value over the interval $0 \le z \le H$ corresponds with the value of p_s from equation (66).

Evaluation of this averaging integral yields

$$p_s \equiv \frac{1}{H} \int_0^H dz\, p_s(z) = A\, E_2(\beta\phi) \tag{70}$$

where E_2 is the exponential integral function defined as

$$E_2(X) = \int_1^\infty dt\, e^{-xt}/t^2 \tag{71}$$

and numerical values of β in the range of $\frac{1}{5}$ to $\frac{1}{7}$ leads to the desired approximate equality

$$E_2(\beta\phi) \approx e^{-\phi} \text{ for } \phi \ll 1. \tag{72}$$

Thus, to make the equation (69) formulation most generally applicable, we define the overall normalization as

$$A \equiv e^{-\phi}\, E_2(\beta\phi) \tag{73}$$

where, as before, $\phi = v_d \cdot \Delta T/H$. Examination of equation (73) using expansions of the E_2 function and for appropriate values of β (for example, $\beta = 1/6$) show that A is always less than unity so that one is never in the embarrassing and puzzling position of having $p_s(z)$ values greater than one.

Another advantage of the equation (69) formulation is that the cumulative survival probability, p_s, after n time steps can be written as

$$\begin{aligned} p_s &= \prod_{i=1}^{n} A \exp\left(-\beta v_d \cdot \Delta T/Z_i\right) \\ &= A \exp\left[-\beta v_d \cdot \Delta t \sum_{i=1}^{n} (1/z_i)\right] \end{aligned} \tag{74}$$

Thus, for computation of a particle's cumulative survival probability it becomes only necessary to accumulate the harmonic sum of individual z_i particle trajectory values, or possibly v_{di}/z_i values if the deposition velocity varies sufficiently rapidly in space or time. Actual evaluation of equation (74) further demands that values of $z_i > H$ be excluded from the sum and that $z_i = 0$ values be replaced with small positive values, perhaps of order $10^{-3} \cdot H$ for a typical $H = 20\ m$.

A further advantage of the proposed formulation is that there are no remaining unspecified time, length, or velocity scales to contend with. Finally, we note that since mathematical particles are never eliminated, the same entity can simultaneously represent physical particles from a range of particle size

categories (not strongly influenced by gravitational settling). It is only necessary to track values of survival probability separately for different v_d values.

3.3 Point and Path-Integrated Concentration Computations

Computation of instantaneous point and path-averaged concentrations requires the "counting" of particles within a volume region about the point or path of interest. These volumetric sampling regions may either be defined in a "box car" sense, with particles within the box being assigned a weight of one and those outside assigned a weight of zero, or in a diffuse volume sense where particles are assigned a continuum of weights depending on their proximity to the actual sampling location. A simple example of the latter concept involves the second-dimensional or third-dimensional Gaussian weighting function

$$w(r) \equiv \frac{1}{(\sqrt{2\pi}\ \sigma)} \cdot \exp\left\{-\frac{1}{2} r^2/\sigma^2\right\}, \tag{75}$$

where r is the scalar distance between the particle and sampling line (n=2) or point (n=3) and $\sqrt{2\pi\sigma}$ is the equivalent box normalization length scale. In the case of the line integral, the length of the finite line, L, will serve as the third dimensions for defining the volume of the cylindrical region. For $L \geq \sqrt{2\pi\sigma}$ the volume associated with the line integration will exceed that associated with the point sample, leading typically to a greater number of sampled particles and consequently a lower statistical uncertainty associated purely with sample size, N. This statistical uncertainty, σ_c, is simply obtained from the theory of Poisson statistics and yields the fractional uncertainty

$$\frac{\sigma_c}{N} \approx 1/\sqrt{N} \quad for \gg 1 \tag{76}$$

for particles with uniform weights w_i. For a mixture of weights, the effective sample size is smaller than N and is given as

$$\frac{\sigma_c}{N} \approx \left[\sum_{i=1}^{N} w_i^2\right]^{1/2} \Bigg/ \sum_{i=1}^{N} w_i \quad for\ N \gg 1 \tag{77}$$

The implication of equation (76) is that to reduce the statistical counting uncertainty to say 10 percent, one must count 100 particles (or more if w_i vary) within the sampling volume. These considerations place a strong constraint on the total number of particles which must be released to achieve a given level of uncertainty. Attempts to reduce computation time by limiting the number of particles lead one to increase the sampling volume length scales, s and L; however, increasing these scales is tantamount to reducing the spatial resolution of the model.

The above methodology is very nearly equivalent to the kernel sampling methods developed by Lorimer (1986) and others, except that the spatially diffuse weighting function (for example, that of equation (75) for n=3) is now attached to each moving particle rather than the sampler. In kernel theory the length

scale, σ, is allowed to grow in time with a growth rate and law which may encompass varying fractions of the turbulent eddy spectrum. This is tantamount to ensemble averaging over possible realizations for that fraction of the turbulent spectra included and may create difficulty in interpreting results especially when a hybrid turbulent parameterization (for example, KS theory plus the Langevin equation) is implemented. Yamada and Bunker's (1988) kernel estimator in the RAPTAD model utilizes the full spatial σ values from Taylor's (1921) homogeneous theory and therefore will yield results as highly smoothed as those resulting from a Lagrangian puff model.

4. DEVELOPMENT AND TESTING OF A PROTOTYPE MODULE

4.1 Driver Program and Mean Flow Trajectory Module

Referring back to figure 1 it is evident that a main driver program is needed to:

- read model control files;
- access meteorological data files and additional external data files;
- serve as an envelope for modules for
  - source characterization and particle release,
  - synthetic KS turbulence field creation, temporal evolution and sampling,
  - particle trajectory simulation,
  - particle deposition and removal,
  - point and path integrated instantaneous and averaged concentrations, and
  - multispectral transmission attenuation; and
- produce appropriate statistical summary and graphical output files.

A basic driver program has been developed and tested. The present version reads the basic model control files, reads gridded hourly fields of mean winds (that is, third-dimensional fields of u, v, w) and other meteorological variables (for example, second-dimensional fields of mixing depth, u_*, w_*, Monin-Obukhov length) generated by the CALMET meteorological model, controls the release of particles from a user-specified source, and generates, stores, updates, and outputs trajectories of particles driven by the mean flow. This driver program also provides a convenient platform for insertion of the above mentioned modules--some of which have been developed and tested separately.

Figure 11 displays the trajectories of five particles released 600 s apart into a CALMET generated surface layer. The particles are tracked for 5 h with arrows indicating particle position and direction every 300 s. In this example, particles respond solely to a local interpolated mean flow determined via bilinear interpolation in x, y, and linear interpolation in z between the

adjacent vertical levels. The interpolation procedures and other discrete operators have, of course, been placed into individual FORTRAN 77 subroutines and functions to yield a readable, structure code.

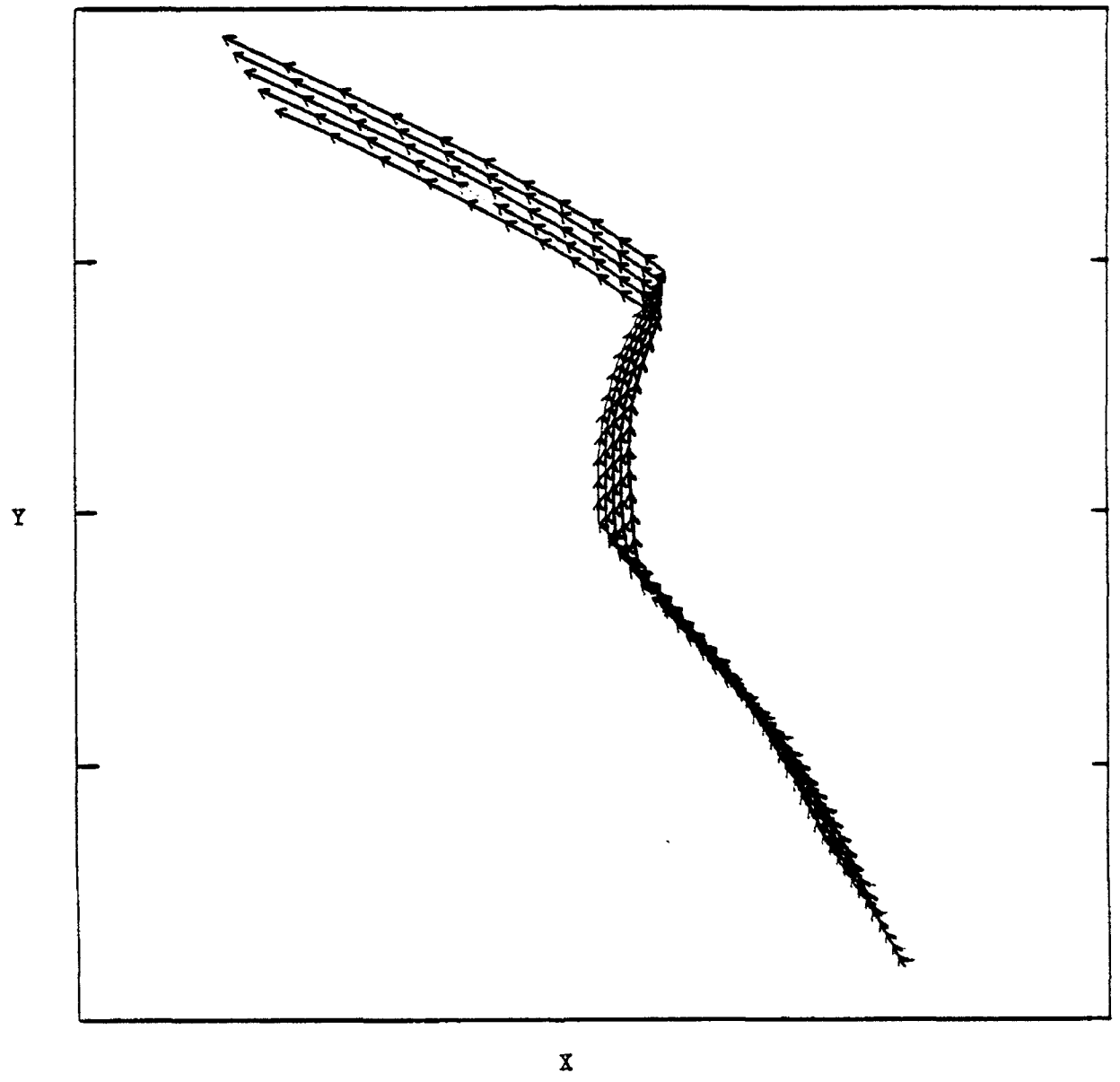

Figure 11. Trajectories of five particles released 600 s apart into a CALMET mesoscale wind field. Arrows depict particle position and direction at 300 s intervals. The x-y region shown is 5 km by 20 km.

The graphical output postprocessor, which generated the x-y plot in figure 11, can also plot the trajectories in other planes. Figures 12 and 13 show the same particle trajectories in the x-z and y-z planes, respectively. As previously noted, particles follow only the interpolated hourly mean wind fields. Thus, all five particles begin on the same trajectory but jump to different trajectories as the next time step's wind fields are utilized. This behavior would be altered by implementing a time interpolation scheme between multiple time levels of winds, but the net effect would still involve an effective "dispersion" of particles due to the particle release time differential.

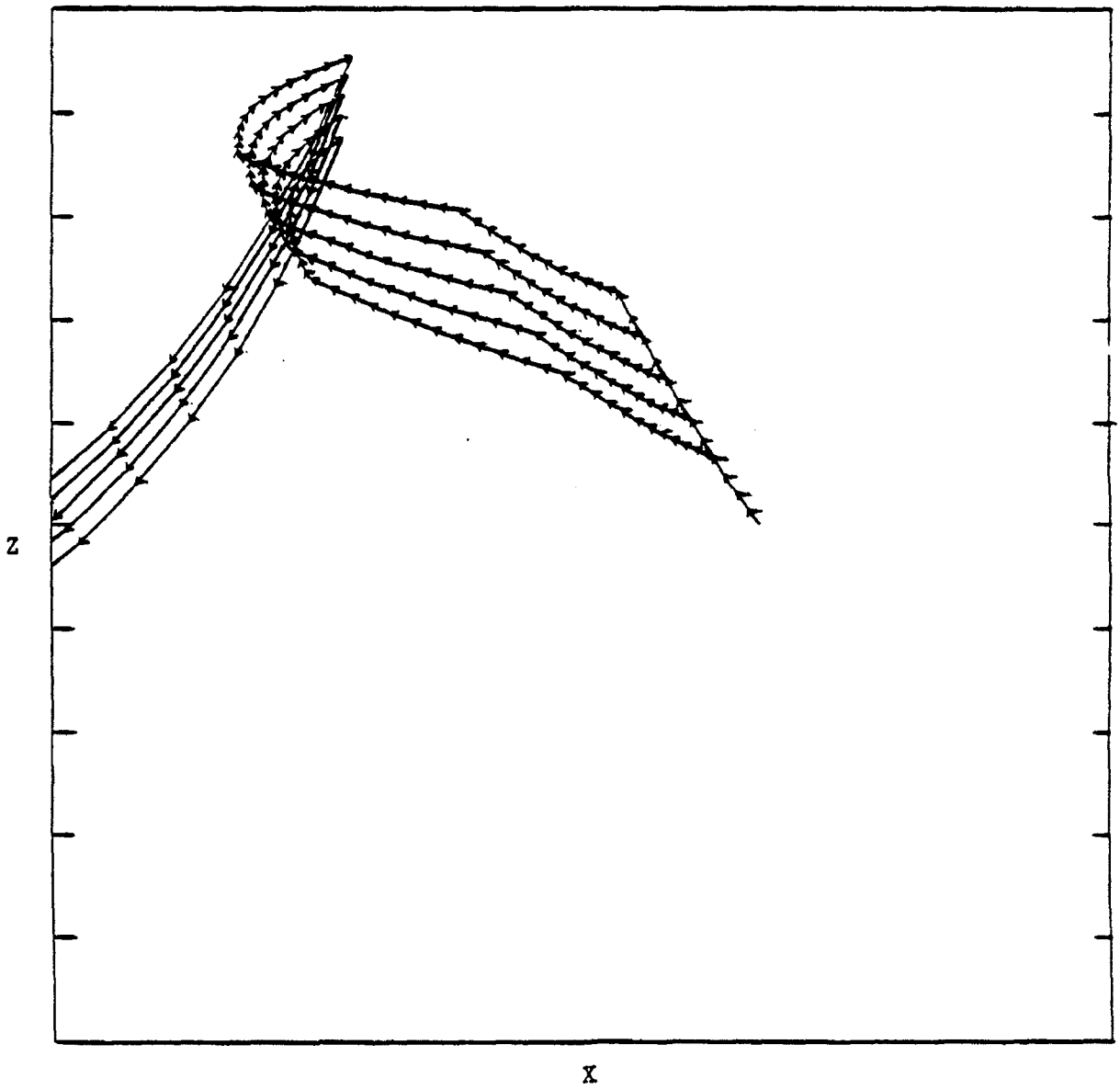

Figure 12. Trajectories of five particles released 600 s apart into a CALMET mesoscale wind field. Arrows depict particle position and direction at 300 s intervals. The x-z region shown is 5 km by 20 m.

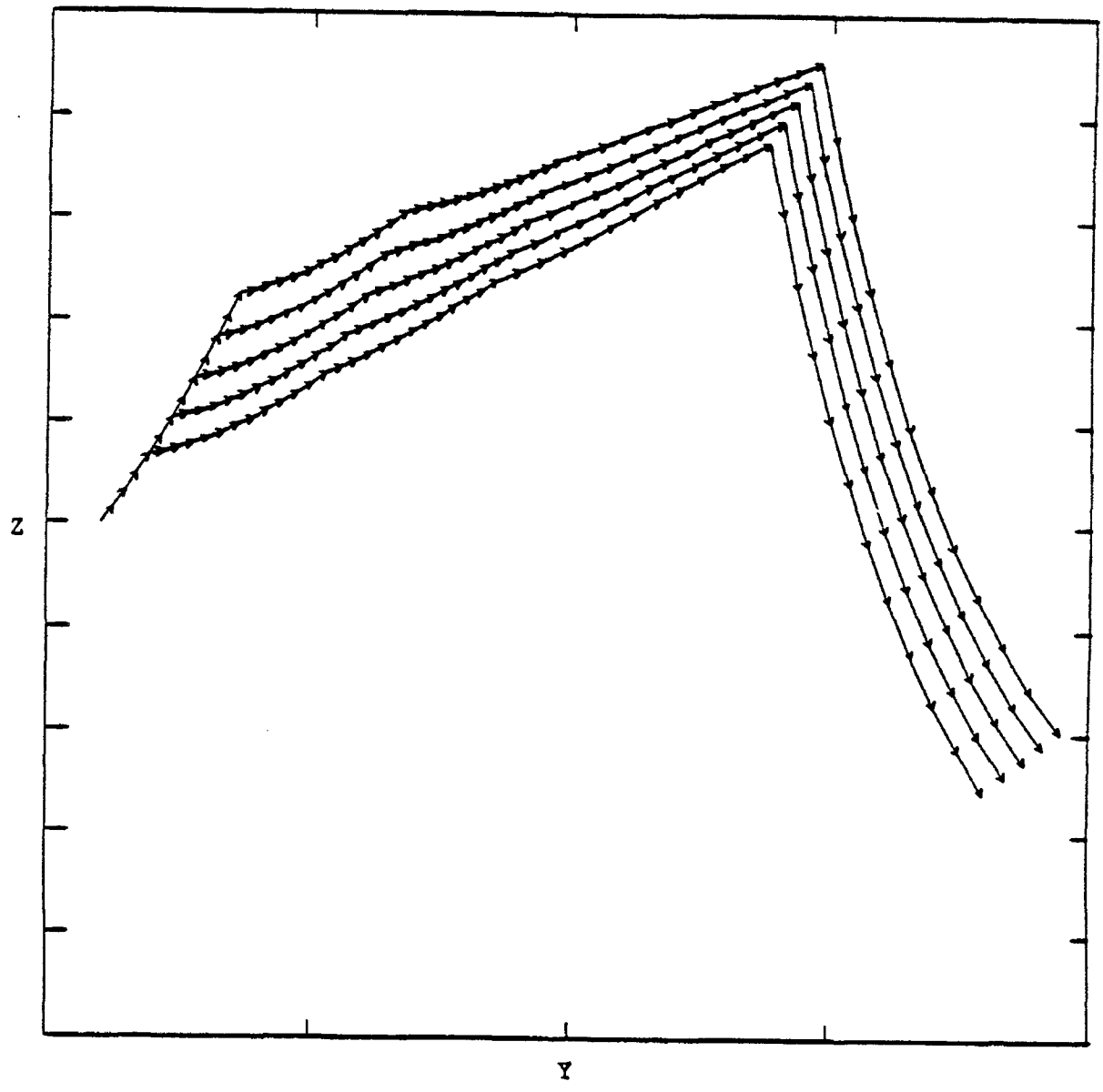

Figure 13. Trajectories of five particles released 600 s apart into a CALMET mesoscale wind field. Arrows depict particle position and direction at 300 s intervals. The y-z region shown is 20 km by 20 m.

4.2 Development and Initial Testing of the Kinematic Simulation Turbulence Module

Individual modules have been developed and tested for the initialization, time advancement, and velocity field sampling of the sub-grid-scale, KS flow fields described in section 2.4. Completely separate KS fields can be generated for each of the mesoscale model's (x, y, z) grid cells (that is, cells denoted by indices i, j, k); however, some meteorological situations such as the convective boundary layer might be more realistically simulated by a single set of KS fields for each x, y (or i, j) column below the mixed layer height.

The KS modules have been conveniently split into the three components of initialization, time advancement, and field sampling so that:

- a field containing N spectral components, with N arbitrary, and user specified spectral shape can be initialized for an arbitrary second-dimensional and third-dimensional mesoscale grid;

- the state of these fields may be stochastically time advanced at any time interval, independent of particle release rate or trajectory increment time steps, with phase evolution factors (that is, the $\underline{u}_{an}$ and T_n of equations (46) and (47) also established in the initialization algorithm; and

- the time analytic values of the components, (u', v', w') may be sampled in space and time as frequently as dictated by the number of particles or other parameters of the problem.

Thus, we have constructed a flexible set of KS velocity field operator functions that can be applied under a wide range of conditions and application circumstances. To date only the equation (44) homogeneous turbulence expressions for an unbounded domain have been included into the algorithms, but transition to an alternative set of equations, such as equations (49) through (51) would only require replacing about 20 lines of code. A "switch" might be ultimately supplied to choose between several KS field formulations.

In the demonstration tests which follow, the objective was to fill a single column of the mesoscale model (that is, with $\Delta x = \Delta y = 5$ km and a boundary layer depth of $\Delta z = 2$ km) with a KS field determined by only five spectral components. These spectral components, chosen to have equal variance and with k values beginning at $2\pi/\Delta x$ (or $2\pi/\Delta z$) and increasing by factors of three for each component, were envisioned as leading to an unrealistic, multi-spiked spectrum of an unphysical nature. A typical time series of sampled u' values every 3 s (for example, figure 14) suggests several dominant frequencies. However, the fixed-point Eulerian power spectra produced during this one hour trial is remarkably smooth beyond the lowest driving frequency and displays a spectral energy falloff exponent of nS(n) in the inertial subrange of somewhat less than 1.0 (for example, = -0.7 *to* -0.8) for u' and w' versus theoretical values of -2/3). These two spectra for u' and w' are displayed as figures 15 and 16, respectively.

Correlograms for these u' and w' time series are displayed in figures 17 and 18, respectively, as a function of time lag. The u' and w' correlograms are remarkably similar, with Lagrangian time scales (same as Eulerian time scales as mean winds were set to zero) of about $T_L = 60$ s.

Unfortunately, the u' data are found to yield a somewhat smaller T_L than that of the w' data; however, this is a direct consequence of the equation (44) formulation of the wind components in terms of a cross product of vectors $\underline{a}$, $\underline{b}$, and $\underline{k}$. Thus, the u' component involves the y and z components of amplitudes $\underline{a}$, $\underline{b}$, whereas the w' velocity involves the x and y components, and attempts to assign the shorter Lagrangian time scale to a_z, b_z amplitudes prove obviously counterproductive. This suggests further that a more direct formulation of the amplitudes (that is, not in terms of cross products), as provided by equations

(49) thru (51), will enable greater control of the spectral and time series characteristics of each of the sub-grid-scale velocity components.

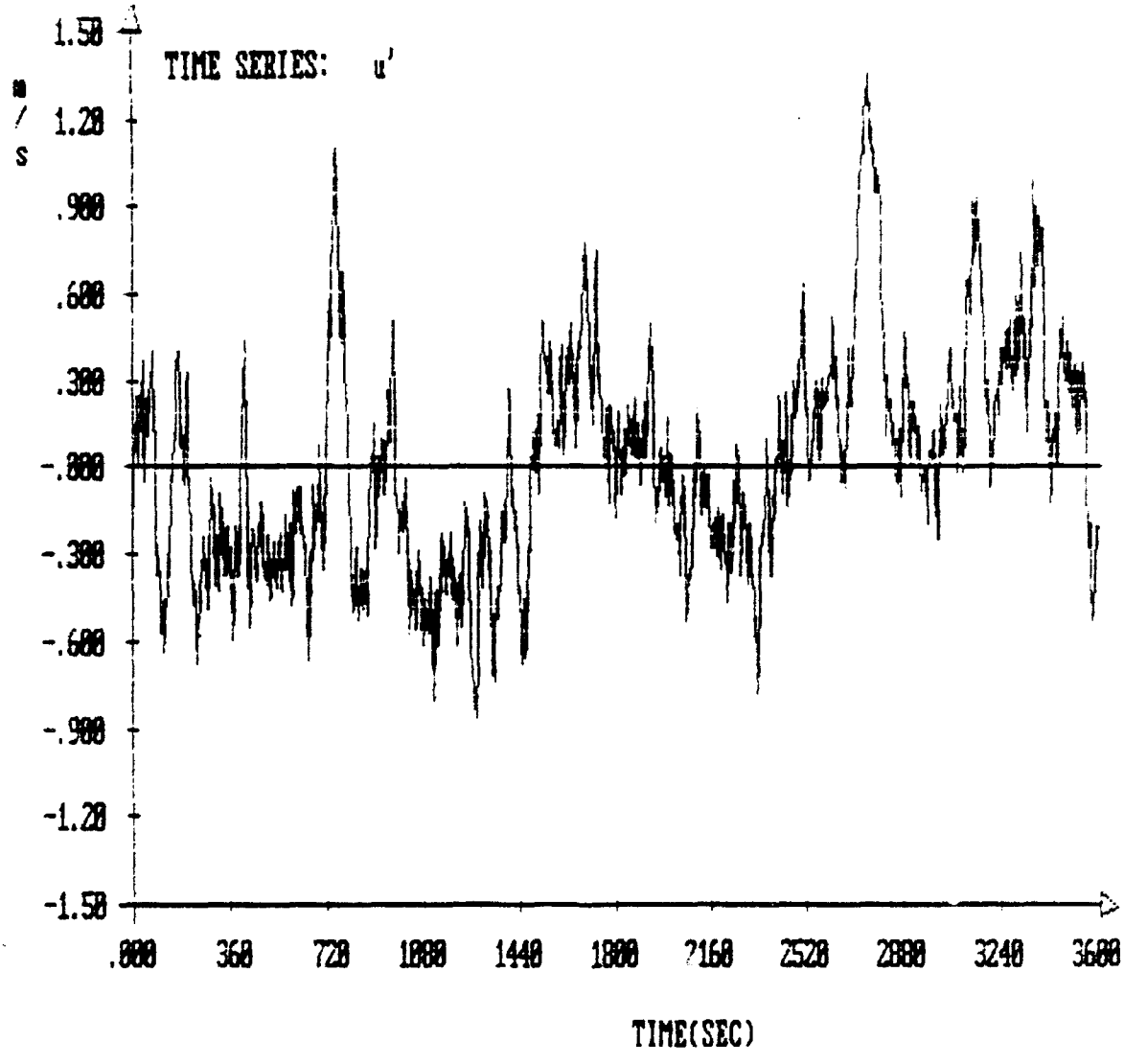

Figure 14. Time series of KS predicted u' velocity fluctuations. The KS amplitude and phase components were advanced every 3 s and the resulting winds sampled at the same time interval.

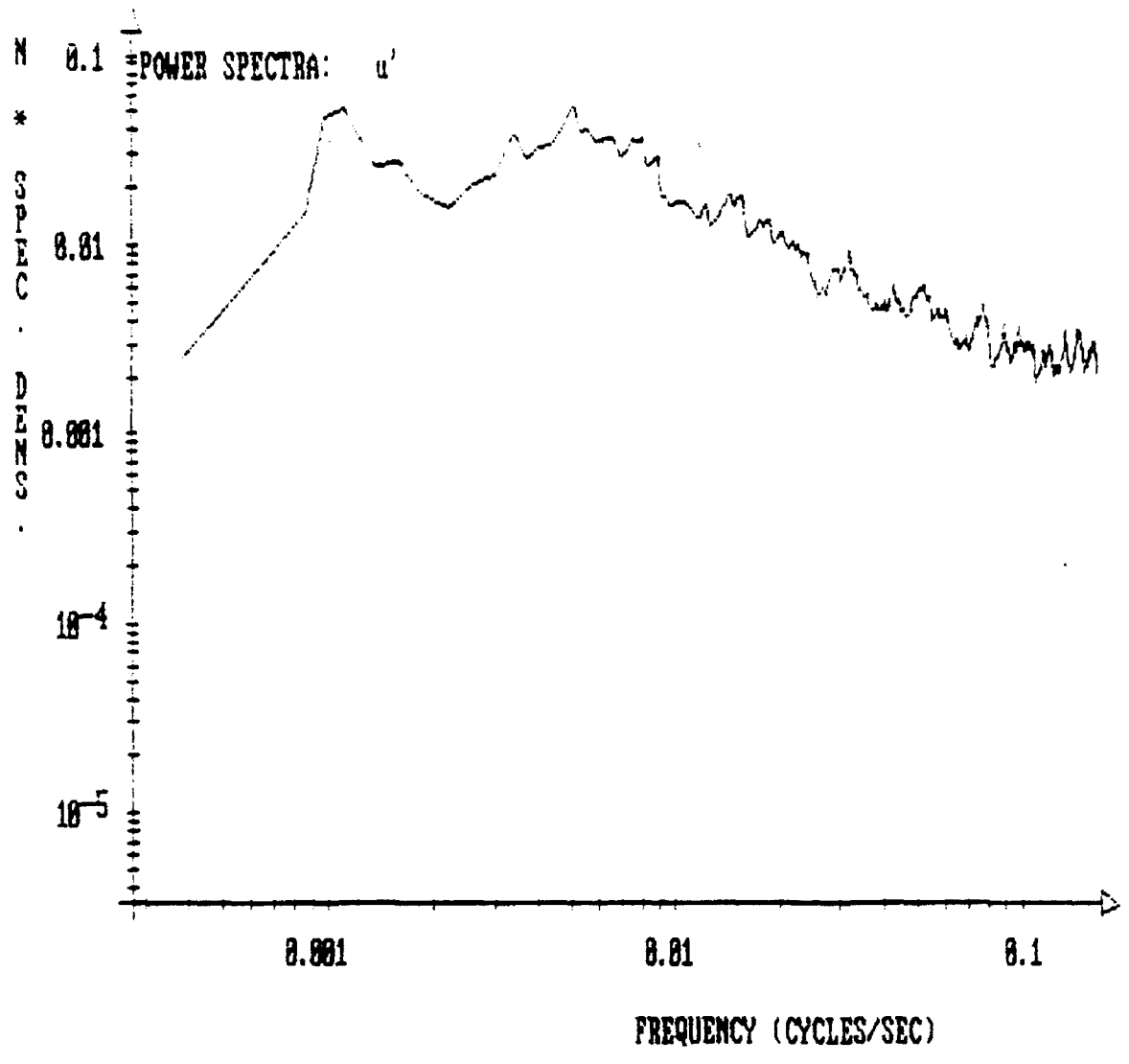

Figure 15. Frequency scaled power spectra, nS(n), for the u' component. The data sample consisted of a 1-h record of KS generated winds with KS field time advancement and sampling intervals of 3 s.

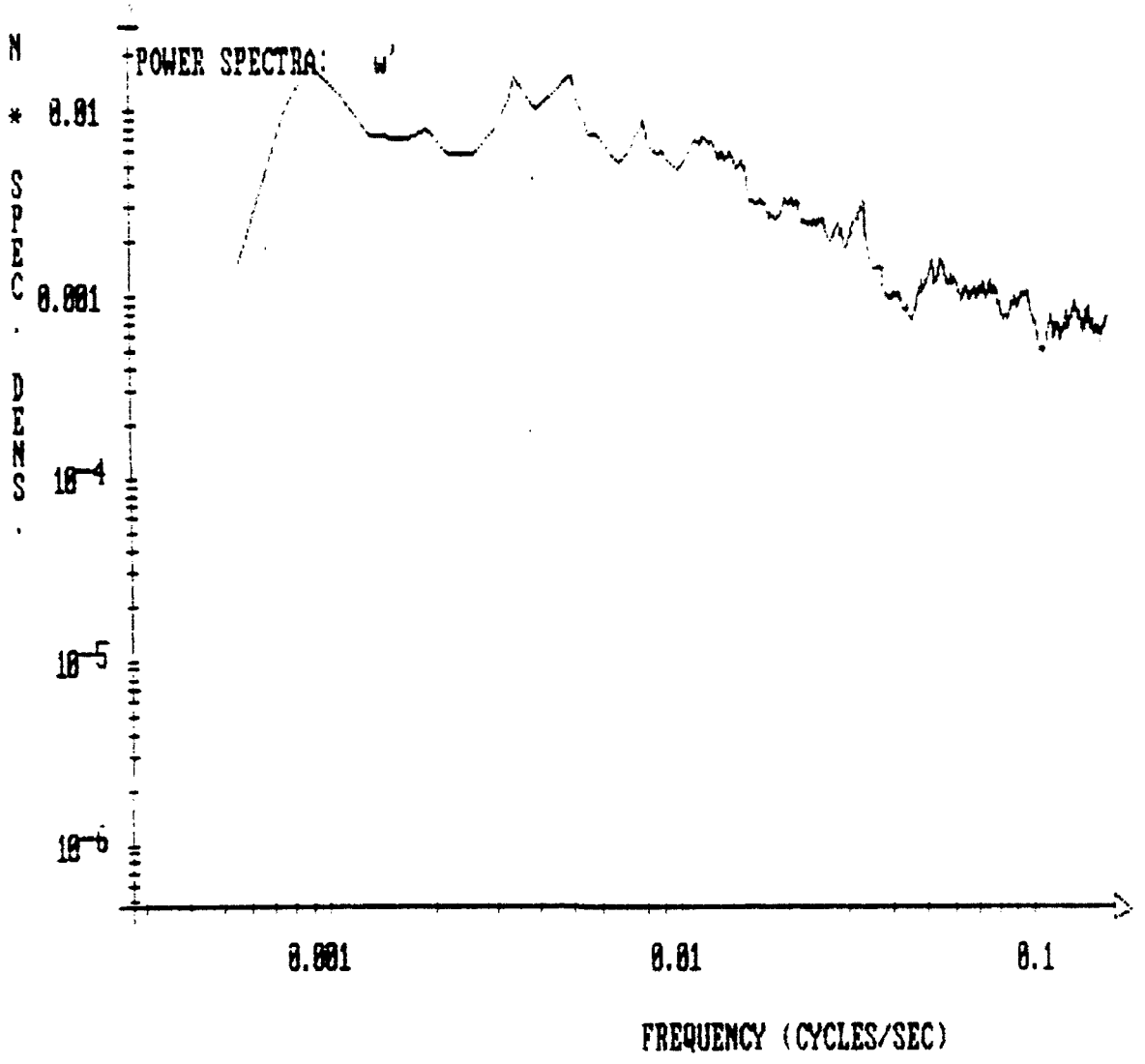

Figure 16. Frequency scaled power spectra, nS(n), for the w' component. The data sample consisted of a 1-h record of KS generated winds with KS field time advancement and sampling intervals of 3 s.

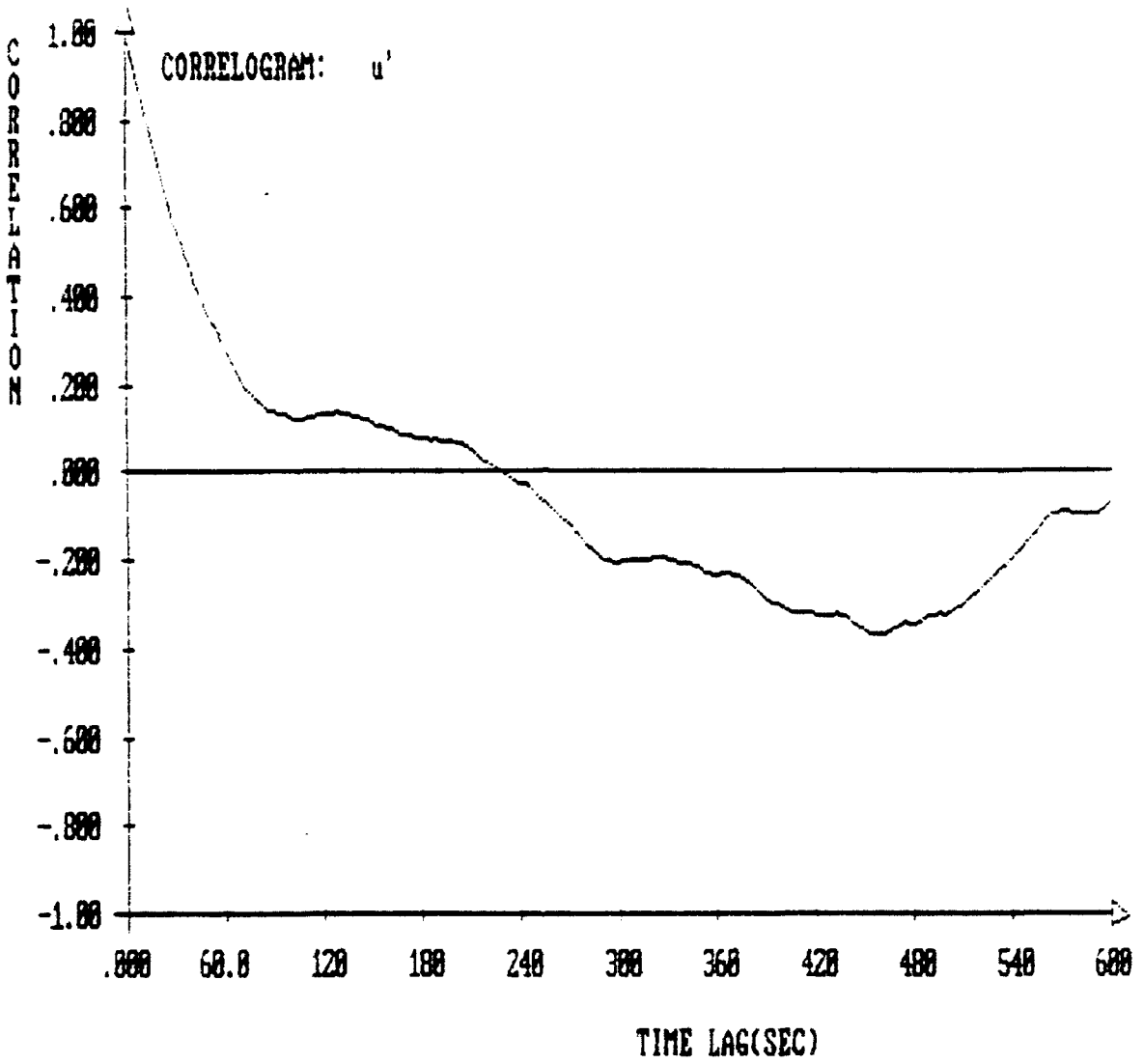

Figure 17. Autocorrelation function for the u' velocity component versus lag time. The data sample consisted of a 1-h record of KS generated winds with KS field time advancement and sampling intervals of 3 s.

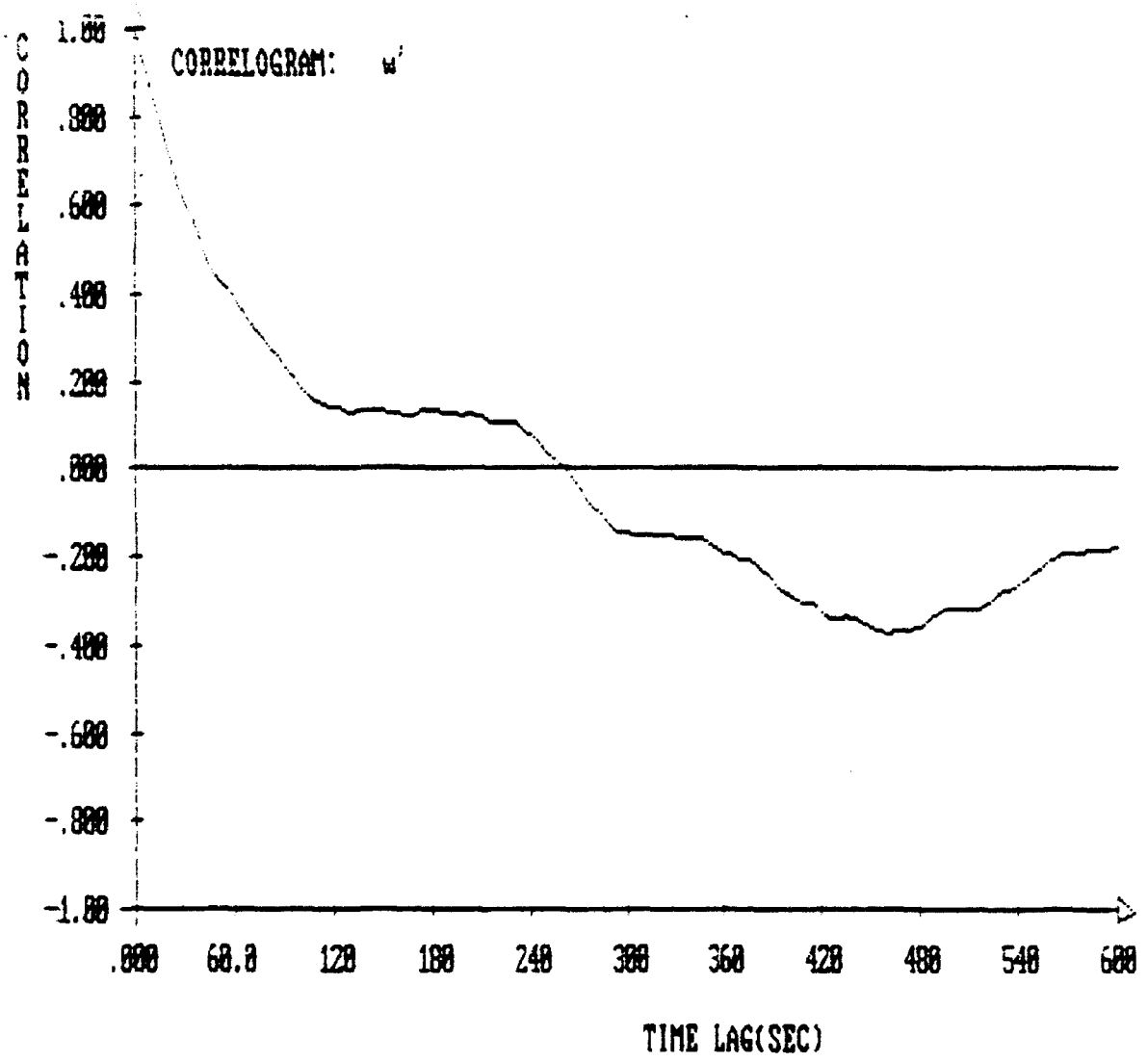

Figure 18. Autocorrelation function for the w' velocity component versus lag time. The data sample consisted of a 1-h record of KS generated winds with KS field time advancement and sampling intervals of 3 s.

Unfortunately, the u' data are found to yield a somewhat smaller T_L than that of the w' data; however, this is a direct consequence of the equation (44) formulation of the wind components in terms of a cross product of vectors $\underline{a}$, $\underline{b}$, and $\underline{k}$. Thus, the u' component involves the y and z components of amplitudes $\underline{a}$, $\underline{b}$, whereas the w' velocity involves the x and y components, and attempts to assign the shorter Lagrangian time scale to a_z, b_z amplitudes prove obviously counterproductive. This suggests further that a more direct formulation of the amplitudes (that is, not in terms of cross products), as provided by equations (49) thru (51), will enable greater control of the spectral and time series characteristics of each of the sub-grid-scale velocity components.

Finally, the above KS winds were used to produce particle trajectories and analyze the dispersion produced by these KS winds alone or in combination with higher frequency turbulence components characterized by a Langevin equation. Figure 19 shows the 1-h trajectory of a single particle driven purely by the KS winds. As a time step of $\Delta t = 3$ s was used for both the KS field update and particle transport, particle position and direction arrows are not shown (that is, as they are not individually distinguishable).

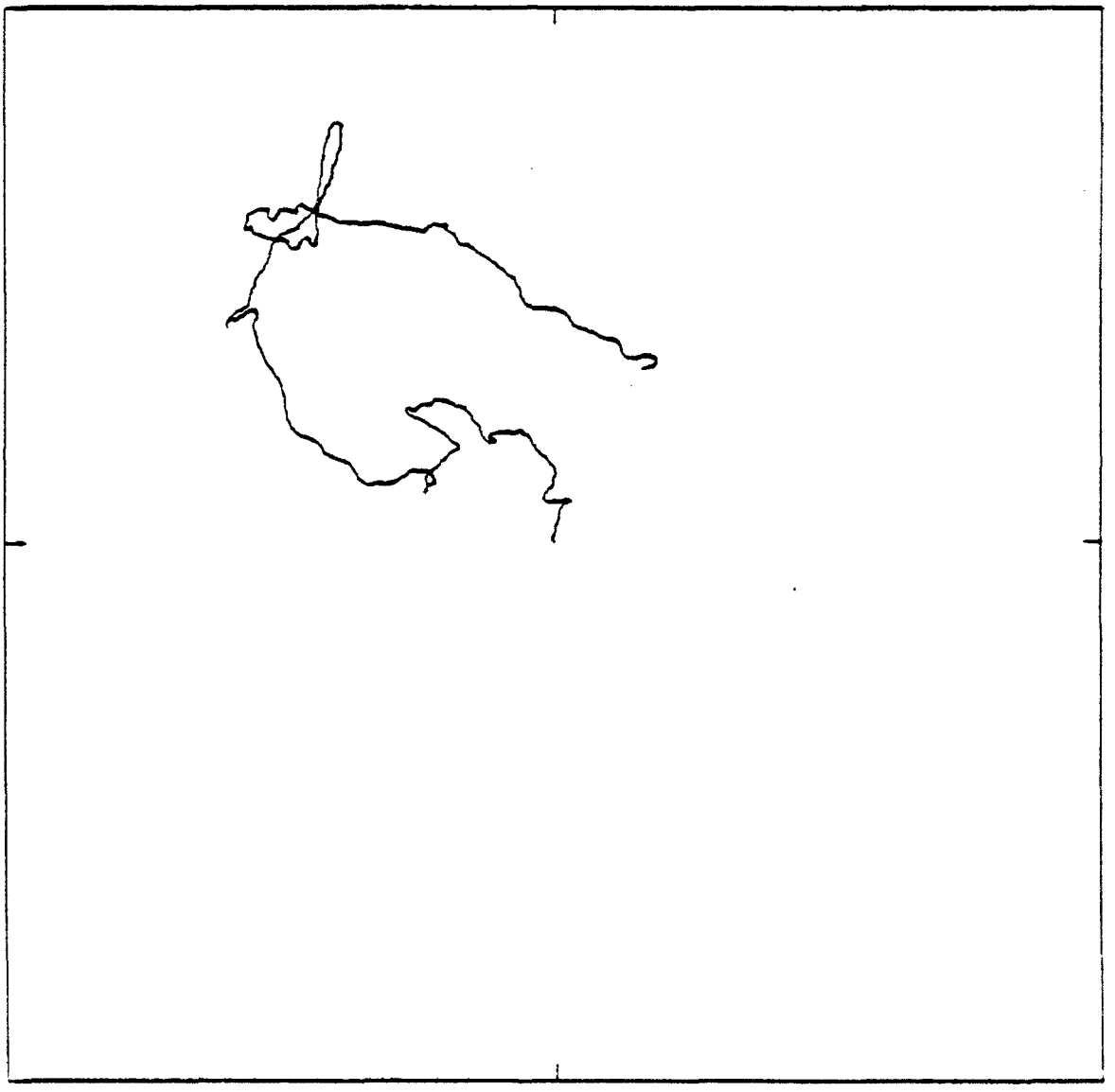

Figure 19. Trajectory of a single particle subjected to the KS generated sub-grid-scale flow fields. The particle trajectory was advanced in time steps of 3 s for 1-h. The x-y region shown is 1 km by 1 km.

When 10 particles were released 3 s apart into the KS winds, interparticle separation grew rather quickly and then leveled off to rather constant values of σ_x, σ_y, and σ_z of 32.3 m, 38.7 m, and 7.95 m, respectively. This termination of the particle cloud's growth is due to the fact that when particles follow pure KS flows they remain on particular evolutionary streamlines and are not able to diffuse across to neighboring streamlines. This was demonstrated by adding a very small, high frequency, homogeneous turbulence component having a velocity standard deviation of only σ = 4.1 cm/s and a Lagrangian time scale of T_L = 1 s. Such a level of turbulence alone would lead to σ_x, σ_y, σ_z = 3.5 m after 1-h, but in combination with the KS flow fields leads to standard deviations of 53.9 m, 46.7 m, and 30 m, respectively. Thus, as anticipated, this very small amount of diffusion caused the particle cloud to grow much larger than computed from the quadrature addition of uncorrelated processes. We also should note that due to the fact that $T_L < \Delta t$ for the fine scale turbulence component, the Langevin equation reduced effectively to the random walk problem so the simpler random walk equation was utilized. In an operational model, a separate Langevin equation would be carried for each particle to maintain complete model generality.

4.3 Additional Modules and Computational Considerations

Section 3.1 describes the results of testing and intercomparing several dry deposition velocity modules for particulates. The algorithm extracted from the most recent version of the Urban Airshed Model (that is, UAM-V) appears to provide reasonable predictions up to particle diameters of about 30 μm, but the work of Noll and Fang (1989) suggests that yet larger particles (for example, up to d_p = 100 μm) may deposit with effective deposition velocities significantly different from that estimated by Stokes law.

Section 3.2 describes a method for assigning survival probabilities or, equivalently, remaining mass fractions to particles that are dry deposited. This approach should be reasonable for those particle sizes whose trajectories are not significantly altered by gravitational settling. For larger particles with more significant gravitational settling velocities, additional tests are required to ensure that the survival probabilities computed via equation (74) do not cause any "double counting" of gravitational settling losses.

A scheme for computing point and path-averaged concentrations based on a modified kernel formulation is discussed in section 3.3. While the simple expression given by equation (75) is easily coded, sensitivity studies of statistical uncertainty versus length scale, σ, and particle release rate should be conducted to ensure a properly engineered model with well understood uncertainty characteristics.

In addition, a complete multispectral transmission/opacity model will ultimately require an electromagnetic scattering module. These exist in a variety of forms ranging from simple optical depth calculations to full, multiple scattering computations for particles having an arbitrary, complex (that is, real and imaginary parts) index of refraction as a function of incident wavelength λ. This topical area was considered beyond the intended scope of the current Phase I effort.

Finally, we note that the original proposal suggested that a RAM disk would need to be utilized to store the large number of particle trajectories anticipated in an operational model. The need arose solely because of the 640K-byte program size limit of the DOS operating environment on personal computers. DOS extenders and/or other operating systems such as UNIX, are now more widely available and will enable all the needed particle trajectory information to be retained within the program provided sufficient physical memory (that is, 4 to 12 mbar) is available. This alternative will be several times faster than a RAM disk and orders of magnitude faster than the use of a hard disk for this function.

5. CONCLUSIONS AND RECOMMENDATIONS

The feasibility of developing a four-dimensional, (for example, space and time varying) non-Gaussian, mesoscale model for multispectral smoke assessments has been evaluated. The basic approach is not unlike that suggested by Ohmstede and Stenmark (1980) except that the advent of kinematic simulation (KS) now enables one to develop nondivergent, sub-grid-scale (SGS) flow/turbulence fields that evolve in time so that true snapshots in time of particle distributions may be obtained in contrast to the ensemble average measures obtainable from use of the Langevin equation to emulate all the subgrid scales of turbulence.

The basic findings of this study include:

(a) Adequate information about the convective boundary layer is available from analyses of field data plus LES data bases to construct the appropriate SGS velocity fields thru kinematic simulation.

(b) Available information on turbulence in the stable boundary layer and that associated with SGS obstacles is less complete but is sufficient for developing the SGS velocity field parameters needed by the KS approach.

(c) The KS approach of Fung et al. (1990) has been tested for velocity fields appropriate for homogeneous turbulence in an unbounded domain. The methodology achieves the desired basic objectives, but modified fields are needed for inhomogeneous turbulence in an environment bounded by the ground. A plausible set of KS field equations have been developed during this study and are given by equations (49) through (51); however, they have not been tested.

(d) Several deposition velocity algorithms for particles have been tested and the resistance based model contained within the UAM-V is recommended for inclusion in the multispectral smoke model. Additional work may be required to adequately model deposition velocities for particles larger than 30 μm in diameter.

(e) A model for assigning survival probabilities to individual particles to account for surface removal has been developed during this study. Equation (74) presents this model which is a function of deposition velocity, time step, the harmonic mean height above terrain, and the depth of the lowest model layer over which deposition removal can occur. The new model should be evaluated, particularly for larger particle sizes where the particle's trajectory is significantly influenced by gravitational settling.

(f) Particles are transported by a wind velocity that is a composite of the mesoscale mean flow, the KS flow associated with the resolved scales of turbulence, and a Langevin equation generated component associated with the finer scales of turbulence that cannot be economically accounted for by the KS representation.

(g) A modified "kernel" method is proposed for computing point and path averaged concentrations as a function of particle size. A smoothing kernel with a time-independent length scale centered on the sampling point or line, rather than centered on the particles, is envisioned as the method which will be most compatible with the overall modeling objective of obtaining instantaneous snapshot measures rather than ensemble or time average measures. This straightforward sampling methodology does not require significant testing but should be engineered to reflect tolerable levels of statistical uncertainty given an operational design level number of particle trajectories.

The work performed during this Phase I effort has provided a number of discrete modeling components along with some very specific areas, as mentioned above, for improving these components. Nevertheless, the completion of an operational model as depicted in figure 1 will require additional developmental work.

One major future work area involves improvement of the linkage between the current parameterizations of turbulence, as discussed in sections 2.1 and 2.2., and the KS parameters of section 2.4. Fung et al. (1990) give some guidance on the partitioning of energy into various spectral components and consider plausible spectral shapes; however, the results of our section 4.2 KS tests show that the energy spectrum resulting from KS modeling is significantly different from the assumed input spectrum. This is because the random components of amplitude and phase generate higher and lower frequency components. In fact, the synthesized spectra contain energy at frequencies all the way to the Nyquist cutoff. Beyond a trial and error approach or an approach involving iterative nonlinear optimization, we need to develop a clearer understanding of the linkage between input and output KS spectra. This is also necessary if we are to understand how much energy and what frequency range should be accounted for by the Langevin particle motion component of section 2.3. Perhaps only those frequencies beyond the KS field advancement frequency need be represented by the Langevin equation.

A Phase II effort to produce an operational scheme should also be governed by clear guiding considerations such as:

- The completed model should be easy to operate and its predictions straightforward to interpret. The operational model should be able to run on time scales of minutes on a 386/486 generation personal computer with 4-16 MB of physical memory.

- The completed model should function on a variety of computer platforms with various operating systems. The current FORTRAN 77 programs can run under DOS or UNIX; however, it may be necessary to recode the algorithms into Ada and perform graphics functions under XWindows to achieve maximum compatibility with DoD standards.

- The completed model should produce a variety of useful statistical and graphical outputs. As instantaneous snapshot quantities are computed, it would seem reasonable to archive the entire probability density distribution of predictions in addition to the time-averaged moment quantities.

Finally, an operational model should be designed to interface to modules and models developed or used by the U.S. Army. For example, the current prototype accesses wind and meteorological fields produced by the CALMET model. This interface should be kept relatively general so that meteorological models possibly better suited to the Army's needs, can be easily accessed. Another clear example of desired flexibility involves the atmospheric optics module. A multispectral radiative transfer or opacity model is needed to convert the concentration predictions into atmospheric transmissions at various wavelengths. This module has not been addressed during this Phase I study but has been part of other U.S. Army research programs. Thus, a successful Phase II model development/delivery program will involve a more detailed evaluation of the Army's completed model requirements, an assessment of the desirability of interfacing to available U.S. Army modeling components, as well as completion of the research and development tasks identified above.

LITERATURE CITED

Allwine, K. J., and C. D. Whiteman, 1985, "MELSTAR: A mesoscale air quality model for complex terrain: Volume I--overview, technical description and user's guide," Pacific Northwest Laboratory, Richland, WA.

Arya, S. P. S., 1984, "Parametric relations for the atmospheric boundary layer," *Bound Layer Meteorol*, 30:57-73.

Blackadar, A. K., and H. Tennekes, 1968, "Asymptotic similarity in neutral barotropic planetary boundary layers," *J Atmos Sci*, 25:1025-1020.

Briggs, G. A., 1985, "Analytical parameterizations of diffusion: the convective boundary layer," *J Clim and Appl Meteorol*, 24:1167-1186.

Britter, R. E., J. C. R. Hunt, and K. J. Richards, 1981, "Air flow over a two-dimensional hill: studies of velocity speed up, roughness effects and turbulence," *Q. J. R. Meteorol Soc*, 107:91-110.

Businger, J. A., J. C. Wyngaard, Y. Izumi, and E. F. Bradley, 1971, "Flux-profile relationships in the atmospheric surface layer," *J Atmos Sci*, 28:181-189.

Carruthers, D. J., and J. C. R. Hunt, 1990, "Fluid mechanics of airflow over hills: turbulence, fluxes, and waves in the boundary layer," *Atmospheric Processes Over Complex Terrain*, W. Blumen, Editor, *Meteorological Monographs*, 23, Number 45, 83-103, American Meteorological Society, Boston, MA.

Carruthers, D. J., J. C. R. Hunt, and W. Weng, 1988, "Computational model of airflow over hills - FLOWSTAR I. Proc. of Envirosoft," *Computer Techniques in Environmental Studies*, P. Zanetti, Editor, Springer-Verlag.

Caughey, S. J., 1981, "Observed characteristics of the atmospheric boundary layer," *Atmospheric Turbulence and Air Pollution Modeling*, F. T. M. Nieuwstadt and H. Van Dop, Editors, D. Reidel Publishing Company, Boston, MA.

Ching, J. K. S., J. M. Godowitch, J. F. Clarke, and A. H. Auer, 1983, "Urban scale variations of turbulence parameters and fluxes," American Meteorology Society Specialty Conference on Air Quality Modeling of the Urban Boundary Layer, Baltimore, MD.

Davis, C. G., B. S. Bunker, and J. P. Mutschlecner, 1984, "Atmospheric transport models for complex terrain," *J Clim Appl Meteorol*, 23:235-238.

Deardorff, J. W., and G. E. Willis, 1975, "A parameterization of diffusion into the mixed layer," *J Appl Meteorol*, 14:1451-1458.

Deardorff, J. W, 1974, "Three-dimensional numerical study of the height and mean structure of a heated planetary boundary layer," *Bound Layer Meteorol*, 7:81-106.

Douglas, S., and R. Kessler, 1988, "User's guide to the diagnostic wind model," (Version 1.0), Systems Applications, Incorporated, San Rafael, CA.

Drummond, I. T., S. Duane, and R. R. Horgan, 1984, "Scalar diffusion in simulated helical turbulence with molecular diffusivity," *J Fluid Mech*, 138:75-91.

Endlich, R. M., F. L. Ludwig, and C. M. Bhumralkar, 1982, "A diagnostic model for estimating winds at potential sites for wind turbines," *J Clim Appl Meteorol*, 21:1441-1454.

Endlich, R. M., 1967, "An iterative method for altering the kinematic properties of wind fields," *J Appl Meteorol*, 6:837-844.

Finnigan, J. J., 1988, "Airflow over complex terrain," *Flow and Transport in the Natural Environment: Advances and Applications*, W. K. Steffer and O. T. Denmead, Editors, Springer-Verlag.

Frost, W., K. H. Huang, and W. M. Farmer, 1982, "Monte Carlo Particle Dispersion (MoCaPD) model for battlefield obscuration studies," Final report, U.S. Army Atmospheric Sciences Laboratory, White Sands Missile Range, NM.

Fung, J. C. H., J. C. R. Hunt, N. A. Malik, and R. J. Perkins, 1990, "Kinematic simulation of homogeneous turbulent flows generated by unsteady random Fourier modes," Submitted to *J Fluid Mech*.

Gifford, F. A., 1982, "Horizontal diffusion in the atmosphere: A Lagrangian-dynamical theory," *Atmos Environ*, 16:505-512.

Goodin, W. R., G. J. McRae, and J. H. Seinfeld, 1980, "An objective analysis technique for constructing three-dimensional urban-scale wind fields, *J Appl Meteorol*, 19:98-108.

Hanna, S. R., J. C. Weil, and R. J. Paine, 1986," Plume model development and evaluation," Report Number D034-500, Electric Power Research Institute, Palo Alto, CA.

Hashem, A., and C. S. Parken, 1991, "A simplified heavy particle random-walk model for the prediction of drift from agricultural sprays," *Atmos Environ*, 25A:1609-1614.

Hicks, B. B., 1985, "Behavior of turbulence statistics in the convective boundary layer," *J Clim Appl Meteorol*, 24:607-614.

Hicks, B. B., 1982, "Critical assessment document on acid deposition," ATDL Contrib. File No. 81/24, Atmospheric Turbulence and Diffusion Laboratory, Oak Ridge, TN.

Hojstrup, J., 1982, "Velocity spectra in the unstable planetary boundary layer," *J Atmos Sci*, 39:2239-2248.

Hunt, J. C. R., R. J. Holroyd, D. J. Carruthers, A. G. Robins, D. D. Apsley, F. B. Smith, and D. J. Thompson, 1990, "Developments in modeling air pollution for regulatory uses," 18th NATO-CCMS International Conference on Air Pollution Modeling and its Applications, Vancouver, Canada, 1-48.

Hunt, J. C. R., S. Leibovich, and K. J. Richards, 1988a, "Turbulent shear flow over hills," *Quart J Roy Meteorol Soc*, 114:1435-1470.

Hunt, J. C. R., and K. J. Richards, 1984, "Stratified air flow over one or two hills," *Boundary-Layer Meteorol*, 30:223-259. [Also in H. Kaplan and N. Dinar, Editors, *Proc. 29th Oholo Biological Conference on Boundary Layer Structure: Modeling and Application to Air Pollution and Wind Energy*, Zichron Ya'Acov, Israel.]

Hunt, J. C. R., 1981, "Diffusion in the stable boundary layer," *Atmospheric Turbulence and Air Pollution Modeling*, F. T. M. Nieuwstadt and H. van Dop, Editors, D. Reidel Publishing Company, Boston, MA.

Hunt, J. C. R., and W. H. Snyder, 1980, "Experiments on stably and neutrally stratified flow over a model three-dimensional hill," *J Fluid Mech*, 96:671-704.

Jackson, P. S., and J. C. R. Hunt, 1975, "Turbulent wind flow over a low hill," *Quart J Roy Meteorol Soc*, 101:929-955.

Janicke, L., 1990, "Ausbreitungsmodell LASAT-C: Handbuch Version 1.00. Primelweg 8, D-7770 Uberlingen. (In German)

Janicke, L. 1985, "Particle simulation of dust transport and deposition and comparison with conventional models," *Air Pollution Modeling and its Application IV*, editor, C. de Wispelaere, Plenum Press, NY.

Janicke, L., 1981, "Particle simulation of inhomogeneous turbulent diffusion," *Proc. of the NATO/CCMS 12th International Technical Meeting on Air Pollution Modeling and its Application*, Menlo Park, CA.

Kaimal, J. C., J. C. Wyngaard, D. A. Haugen, O. R. Cote, and Y. Yzumi, 1976, "Turbulence structure in the convective boundary layer," *J Atmos Sci*, 33:2152-2169.

Kaimal, J. C., 1973, "Turbulence spectra, length scales and structure parameters in the stable surface layer," *Bound Layer Meteorol*, 4:289-309.

Kaimal, J. C., J. C. Wyngaard, Y. Yzumi, and O. R. Cote, 1972, "Spectral characteristics of surface-layer turbulence," *Quart J Roy Meteorol Soc*, 98:563-589.

Kraichnan, R. H., 1970, "Diffusion by a random velocity field," *Phys Fluids*, 13:22-31.

Lamb, R. G., 1981, "Diffusion in the convective boundary layer," *Atmospheric Turbulence and Air Pollution Modeling*, T. F. M. Nieuwstadt and K. van Dop, editors, D. Reidel Publishing Company, Boston, MA.

Legg, B. J., and M. R. Raupach, 1982, "Markov-chain simulation of a particle dispersion in inhomogeneous flows: the mean drift velocity induced by a gradient in Eulerian velocity variance," *Bound Layer Meteorol*, 24:3-13.

Ley, A. J., and D. J. Thomson, 1983, "A random walk model dispersion in the diabatic surface layer," *Quart J Roy Meteorol Soc*, 109:847-880.

Liu, M. K., and M. A. Yocke, 1980, "Siting of wind turbine generators in complex terrain," *J Energy*, 4:10-16.

Lorimer, G. S., 1986, "The kernel method for air quality modeling: I. Mathematical foundation," *Atmos Environ*, 20:1447-1452.

Ludwig, F. L., J. M. Livingston, and R. M. Endlich, 1991, "Use of mass conservation and critical dividing streamline concepts for efficient objective analysis of winds in complex terrain," *J Appl Meteorol* (to appear).

Ludwig, F. L., and R. M. Endlich, 1988, "User's guide for the winds on critical streamline surfaces (WOCSS) code," Final report, U.S. Army Contract DAAL-03-D-86-0001/680, SRI International, Menlo Park, CA.

Mallier, R., and M. Maxey, 1991, "The settling of nonspherical particles in a cellular flow field," *Phys Fluids*, A3:1481-1494.

Mattocks, C. A., J. W. Zack, and M. D. Bousquet, 1989, "A three-dimensional mesoscale atmospheric simulation system for use in various mobile battlefield environments, Phase I: demonstration of feasibility," Report No. CR-89-0059-1, U.S. Army Atmospheric Sciences Labortary, White Sands Missile Range, NM.

Moeng, C. H., and J. C. Wyngaard, 1988, "Spectral Analysis of Large-Eddy Simulation of the Convective Boundary Layer," *J Atmos Sci*, 45:3573-3587.

Moller U., and G. Schumann, 1970, "Mechanisms of transport from the atmosphere to the earth's surface," *J Geophys Res*, 75:3013-3019.

Moraes, O. L. L., 1988, "The velocity spectra in the stable atmospheric boundary layer," *Bound Layer Meteorol*, 43:223-230.

Moraes, O. L. L., and M. Epstein, 1987, "The velocity spectra in the stable surface layer," *Bound Layer Meteorol*, 40:407-414.

Nieuwstadt, F. T. M., 1984, "Some aspects of the turbulent stable boundary layer," *Bound Layer Meteorol*, 30:31-55.

Nieuwstadt, F. T. M., and H. van Dop, 1982, *Atmospheric Turbulence and Air Pollution Modeling*, Raidal, 358 pp.

Noll, K. E., and K. Y. P. Fang, 1989, "Development of a dry deposition model for atmospheric coarse particles," *Atmos Environ*, 23:585-594.

Ohmstede, W. D., and E. B. Stenmark, 1980, "A model for characterizing transport and diffusion of air pollution in the battlefield environment. Second Joint AMS/APCA Conference of Applications of Air Pollution Meteorology," American Meteorological Society, Boston, MA.